Arbeitsbericht
NAB 22-03

**TBO Rheinau-1-1:
Data Report**

**Dossier IV
Microfacies, Bio- and Chemo-
stratigraphic Analysis**

June 2023

S. Wohlwend, H.R. Bläsi, S. Feist-Burkhardt,
B. Hostettler, U. Menkveld-Gfeller,
V. Dietze & G. Deplazes

nagra.

Arbeitsbericht
NAB 22-03

**TBO Rheinau-1-1:
Data Report**

**Dossier IV
Microfacies, Bio- and Chemo-
stratigraphic Analysis**

S. Wohlwend[1], H.R. Bläsi[2], S. Feist-Burkhardt[3,4],
B. Hostettler[5], U. Menkveld-Gfeller[5],
V. Dietze[6] & G. Deplazes[7]

[1] Geological Institute, ETH Zurich
[2] Geo-Consulting, Wünnewil, Switzerland
[3] SFB Geological Consulting & Services, Ober-Ramstadt, Germany
[4] Département des Sciences de la Terre, Université de Genève
[5] Natural History Museum Bern
[6] Nördlingen, Germany
[7] Nagra

This NAB aims at reporting drilling results at an early stage. Additional borehole-specific data will be published elsewhere.

In the event of inconsistencies between dossiers of this NAB, the dossier addressing the specific topic takes priority. In the event of discrepancies between Nagra reports, the chronologically later report is generally considered to be correct. Data sets and interpretations laid out in this NAB may be revised in subsequent reports. The reasoning leading to these revisions will be detailed there.

December 2023: Replacement of Tab. 1-2 with an updated version.

Table of Contents

List of Tables

List of Figures

List of Appendices

1 Introduction

1.1 Context

To provide input for site selection and the safety case for deep geological repositories for radio-active waste, Nagra has drilled a series of deep boreholes ("Tiefbohrungen", TBO) in Northern Switzerland. The aim of the drilling campaign is to characterise the deep underground of the three remaining siting regions located at the edge of the Northern Alpine Molasse Basin (Fig. 1-1).

In this report, we present the results from the Rheinau-1-1 borehole located in the siting region Zürich Nordost (Fig. 1-2). In the following, the unique exploration objective of this specific bore-hole is further outlined.
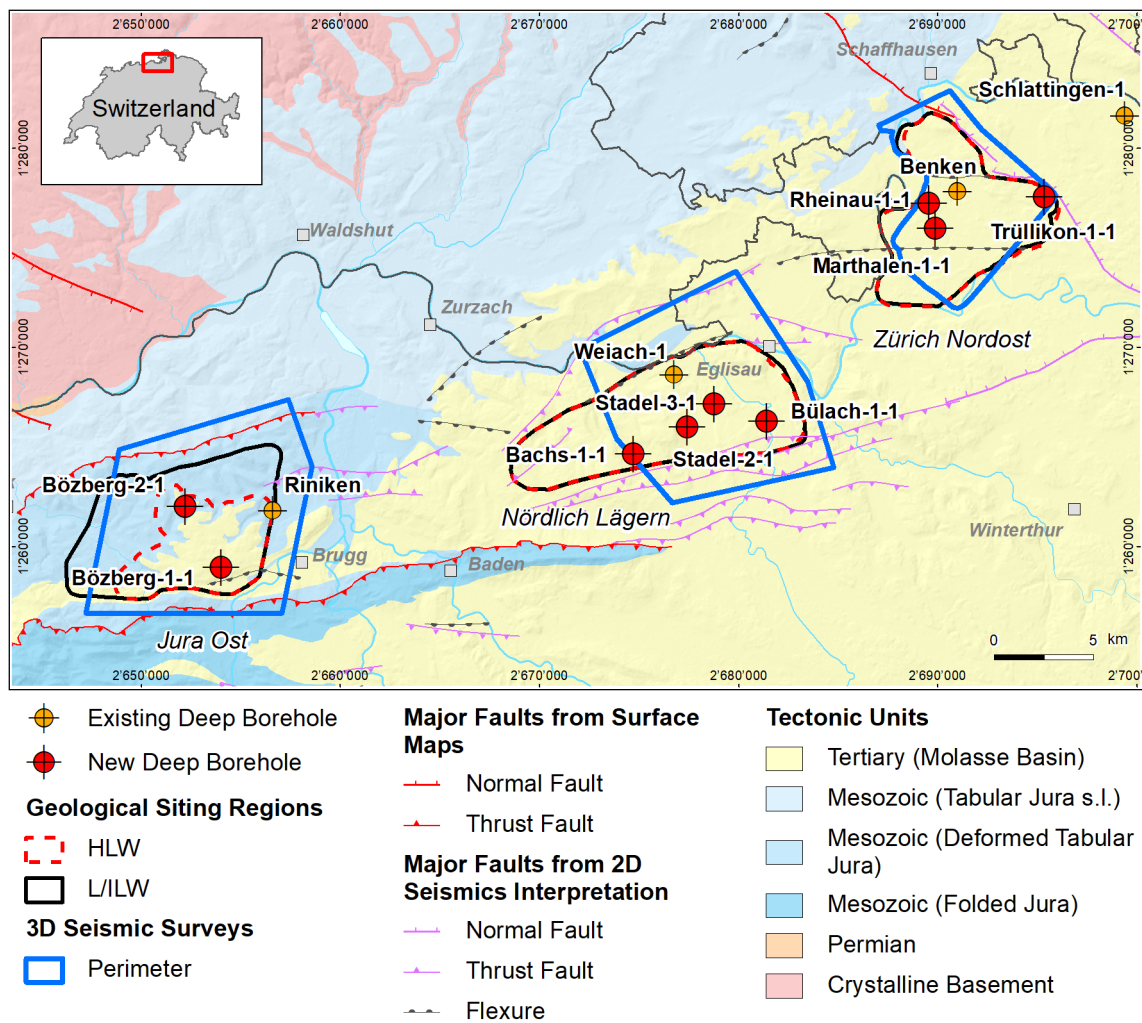
Fig. 1-1: Tectonic overview map with the three siting regions under investigation
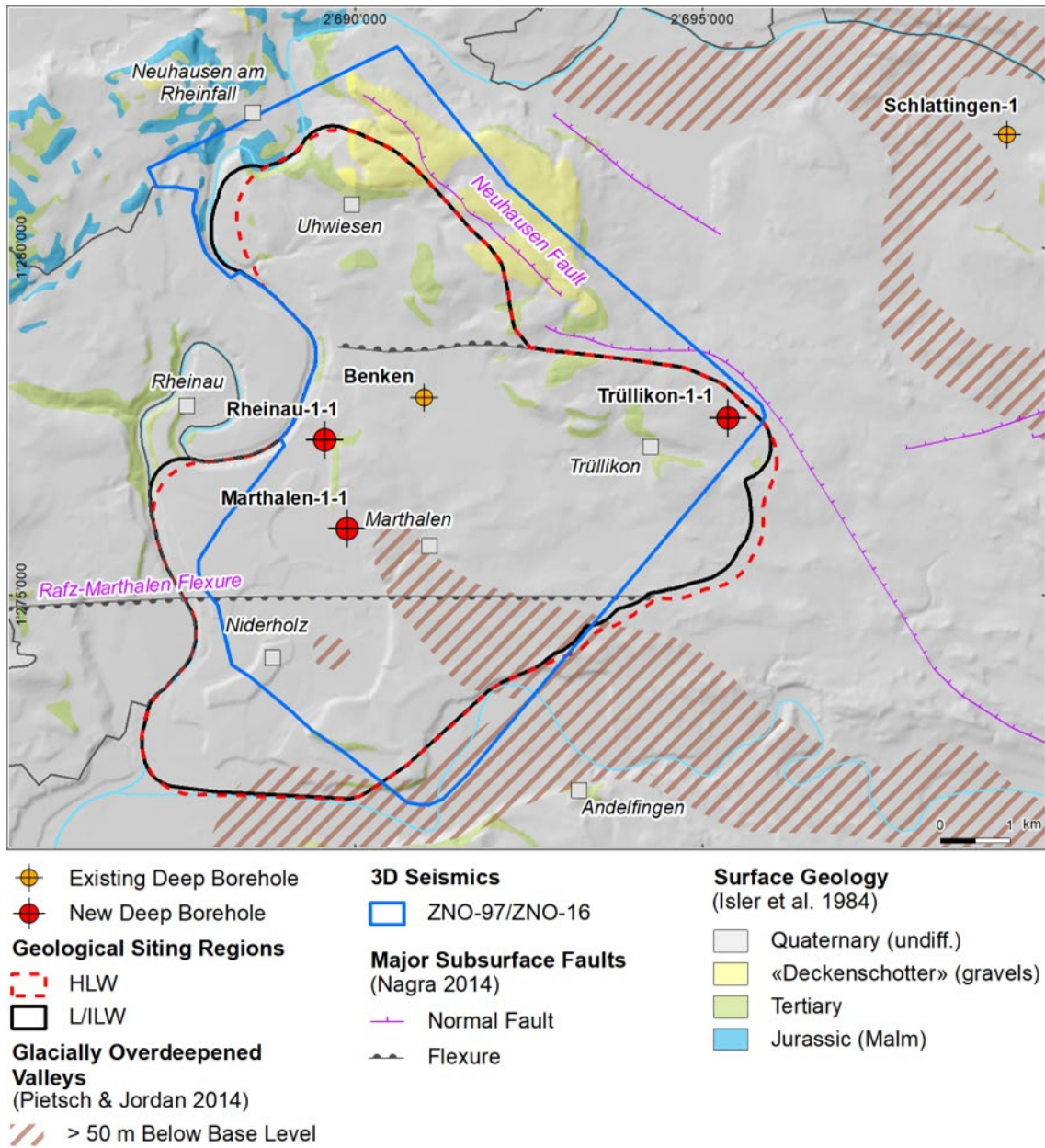
Fig. 1-2:   Overview map of the investigation area in the Zürich Nordost siting region with the location of the RHE1-1 borehole in relation to the Benken, TRU1-1 and MAR1-1 boreholes

Exploration objective of the Rheinau-1-1 borehole

In the context of Nagra's TBO project, the Rheinau-1-1 (RHE1-1) borehole is the only deviated borehole. It was planned as a case study with the primary objective of characterising the structural geology of the Opalinus Clay in the area of a steeply dipping fault. Furthermore, dedicated hydrological packer testing and investigations of natural tracers in porewater were conducted to investigate the self-sealing capacity of the Opalinus Clay. More specifically, a stepped constant head injection test was performed in addition to the standard hydraulic packer test to investigate the evolution of transmissivity as a function of effective stress in a fractured interval (*cf.* Dossier VII, Hydraulic Packer Testing for details).

To enable hydraulic testing in a rock with relatively low strength and high swelling capacity, the
To enable hydraulic testing in the Opalinus Clay with its relatively low strength and high swelling
capacity, the maximum borehole deviation (with respect to vertical) was limited to approximately
35° (borehole plunge of 55°). Hence, for the absolute deviation, a trade-off had to be made
between maximising the lateral coverage for fracture frequency statistics (large deviation desired)
and robust in-situ testing (small deviation desired).

Given the above-outlined scientific goals and related technical requirements, the Rheinau Fault,
located immediately east of the Rheinau-1 drill site, was selected for this case study. It is an NNE-
SSW trending, steeply dipping fault showing only very minor indications of vertical offsets in
seismic amplitude sections. Nevertheless, it was already identified in seismic attribute horizon
slices during initial interpretation of Nagra's 3D seismic campaign in the Zürich Nordost siting
region (Birkhäuser et al. 2001) and later confirmed during the analysis of follow-up seismic
processing products (e.g. Nagra 2019). Fig. 1-3 shows that this fault has a clear seismic attribute
expression along the boundaries of the formations below the Opalinus Clay and also along some
of the more brittle units above (see horizon slices of the Top Bänkerjoch and Top Villigen
Formations shown in Fig. 1-3). However, within the Opalinus Clay, no clear seismic expression
is observed. Fig. 1-4 shows the 3D seismic interpretation considered for trajectory planning of the
RHE1-1 borehole together with the discussed and executed borehole trajectories.
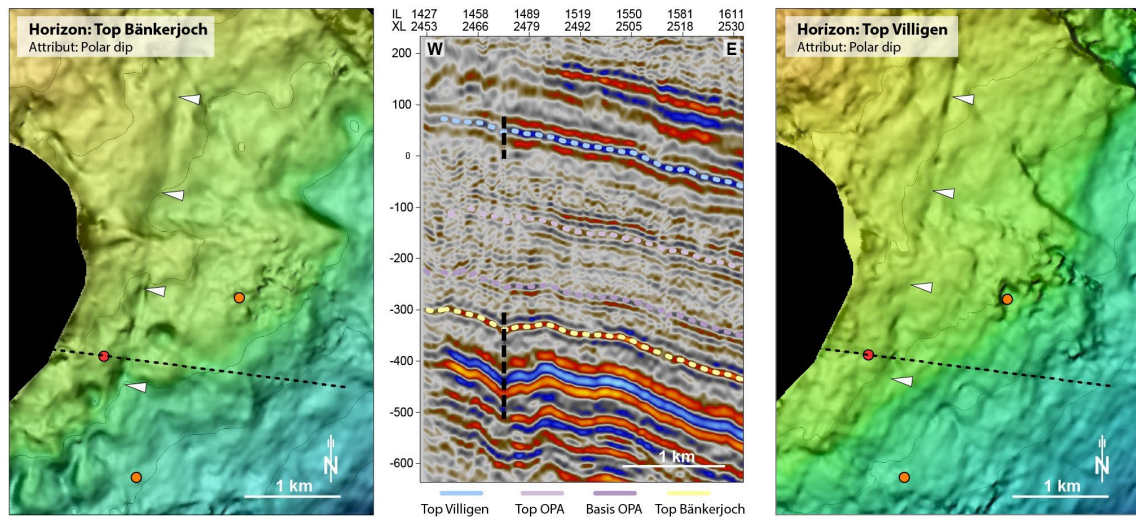
Fig. 1-3:   Seismic amplitude cross-section and seismic attribute maps showing the Rheinau
Fault

Left and right panels: Seismic attribute maps (polar dip) of a depth-migrated seismic cube
(PSDM-A) overlain with depth values (yellowish and blueish colors indicate shallower and
larger depths, respectively). The dashed black line indicates the position of the seismic
section shown in the central panel. Red and orange dots show the position of the RHE1-1
borehole and neighouring boreholes, respectively. White trianlges mark the lineament repre-
senting the Rheinau Fault.

Central panel: Corresponding seismic amplitude section crossing the Rheinau Fault. The
vertical axis indicates depth above sea level, and the horizontal axis shows the inline and
crossline positions. The approximate trace of the Rheinau Fault above and below the
Opalinus Clay is indicated by dashed black lines.
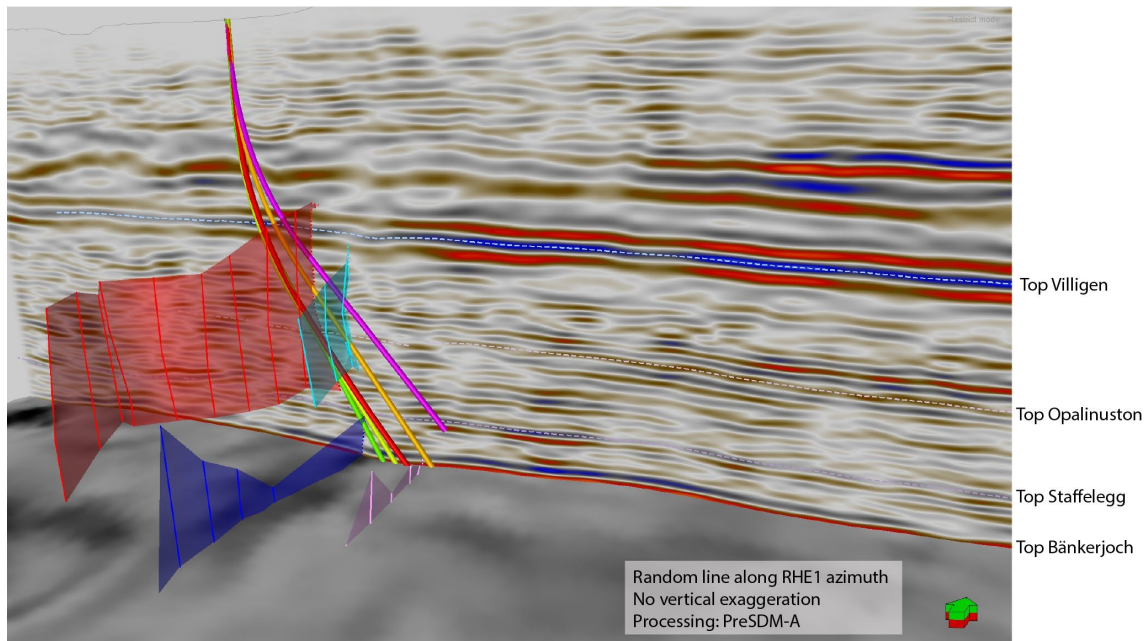
Fig. 1-4: Detailed seismic fault interpretation available for trajectory planning and discussed/ executed well trajectories

Cross-section shows seismic amplitude (seismic processing: pre-stack depth migration PDSM-A). The north direction is indicated by a green-and-red arrow. The vertical distance between the Top Opalinus Clay and Top Staffelegg is ~ 120 m and shows no vertical exaggeration. The horizon slice shows polar dip attribute. Semitransparent subvertical surfaces indicate intepreted faults. The final planned and the drilled trajectories are shown in light green and red, respectively. Other discussed trajectories are shown in yellow, orange and red.

Fig. 1-5 shows a conceptual structural model for the Rheinau Fault incorporating both 3D seismic interpretations and observations from other exploration boreholes as well as from outcrop studies. This conceptual model shows a pronounced mechanical stratigraphy of Northern Switzerland's Mesozoic sedimentary sequence with more focused deformation in the competent units, and distributed deformation in the incompetent units (Roche et al. 2020). Prior to drilling, three hypotheses were formulated on what the RHE1-1 borehole is likely to encounter in the Opalinus Clay. These hypotheses ranged from 1) absence of a distinct fault zone, likely due to a strong degree of strain partitioning within the rheologically weak Opalinus Clay, 2) one or several prominent fault zones, for example revealing cataclastic fault rock or scaly clay as it has been described to occur along larger faults within the Opalinus Clay (Jäggi et al. 2017) and 3) the former but including the occurrence of secondary mineralisations.

As this report represents a data documentation, it deliberately avoids engaging in a synthesis of the observations and test results. Nevertheless, the following results can already be highlighted:

• The drilled trajectory was within close limits compared to the planned well path (see Dossier I for a detailed comparison).

• The borehole did not yield any evidence of a larger-scale fault zone within the Opalinus Clay. However, a number of fault planes have been encountered (*cf.* Dossier V).

• In-situ hydraulic packer tests across these features (*cf.* Dossier VII) yielded hydraulic conductivities similar to undisturbed Opalinus Clay.

- The stepped constant head test demonstrated that a significant enhancement of the flow rate can only be achieved in existing fractures if the fluid pressure is raised considerably and the magnitude of elevated fluid pressure can be maintained (*cf.* Dossier VII).

- Excursions in the profiles of natural tracers can indicate past fluid flow. No such irregularities are seen for the RHE1-1 borehole in the Opalinus Clay (*cf.* Dossier VIII). The stable isotope porewater profiles show characteristics similar to the neighouring vertical boreholes MAR1-1 and Benken.
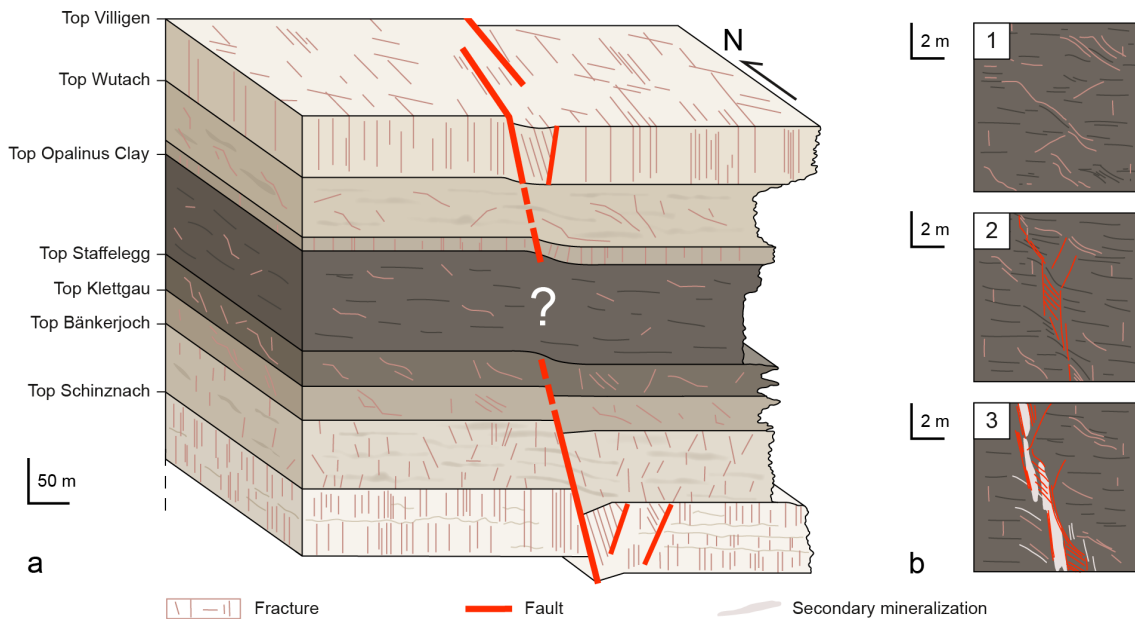
Fig. 1-5:　　Conceptual structural model of the Rheinau Fault

(a) Conceptual block model. The pronounced mechanical stratigraphy of the Mesozoic sequence in the area is stressed via a schematic weathering profile. The RHE1-1 borehole aimed at characterising the deformation style in the Opalinus Clay constituting a mechanically weak layer in between rheologically stiffer units (e.g. under- and overlying Schinznach/ Bänkerjoch and Villigen/Wutach Formations). According to outcrop records and previous borehole results, these units show a significantly higher frequency of fault planes compared to the Opalinus Clay. In 3D seismics, the Rheinau Fault is also only clearly recognisable at the horizons related to stiffer formations.

(b) Hypothetic deformation characteristics of the Opalinus Clay to be encountered in the RHE1-1 borehole: 1) No exceptional deformation features besides small-scale fault planes as previously observed in vertical boreholes outside of seismically recognised faults. 2) One or several localised zones associated with cataclastic fault rock (e.g. scaly clay) as described for larger fault zones elsewhere (e.g. Jäggi et al. 2017). 3) The above, but also including secondary mineralisation (not to scale on picture).

1.2 Location and specifications of the borehole

The Rheinau-1-1 (RHE1-1) exploratory borehole is the eighth borehole drilled within the framework of the TBO project. The drill site is located in the western part of the Zürich Nordost siting region (Fig. 1-2). The deviated borehole reached a final depth of 827.99 m MD = 745.33 m TVD (true vertical depth)[1]. The borehole specifications are provided in Tab. 1-1.

Tab. 1-1: General information about the RHE1-1 borehole

Siting region	Zürich Nordost
Municipality	Rheinau (Canton Zürich / ZH), Switzerland
Drill site	Rheinau-1 (RHE1)
Borehole	Rheinau-1-1 (RHE1-1)
Coordinates	LV95: 2'689'563.92 / 1'277'235.06
Elevation	Ground level = top of rig cellar: 387.23 m above sea level (asl)
Borehole depth	827.99 m measured depth (MD) = 745.33 m true vertical depth (TVD) below ground level (bgl)
Borehole deviation at total depth (TD)	Inclination from vertical: 38.93° Azimuth from North: 76.25°
Drilling period	19th July – 10th October 2021 (spud date to end of rig release)
Drilling company	PR Marriott Drilling Ltd
Drilling rig	Rig-16 Drillmec HH102
Drilling fluid	Water-based mud with various amounts of different components such as[2]: 0 – 497 m: Polymers 497 – 828 m: Potassium silicate & polymers

The lithostratigraphic profile and the casing scheme are shown in Fig. 1-6. The main lithostratigraphic boundaries in the RHE1-1 borehole is shown in Fig. 1-7.

---

[1] Measured depth (MD) refers to the position along the borehole trajectory, starting at ground level, which for this borehole is the top of the rig cellar. For a perfectly vertical borehole, MD below ground level (bgl) and true vertical depth (TVD) are the same. In all Dossiers depth refers to MD unless stated otherwise.

[2] For detailed information see Dossier I.
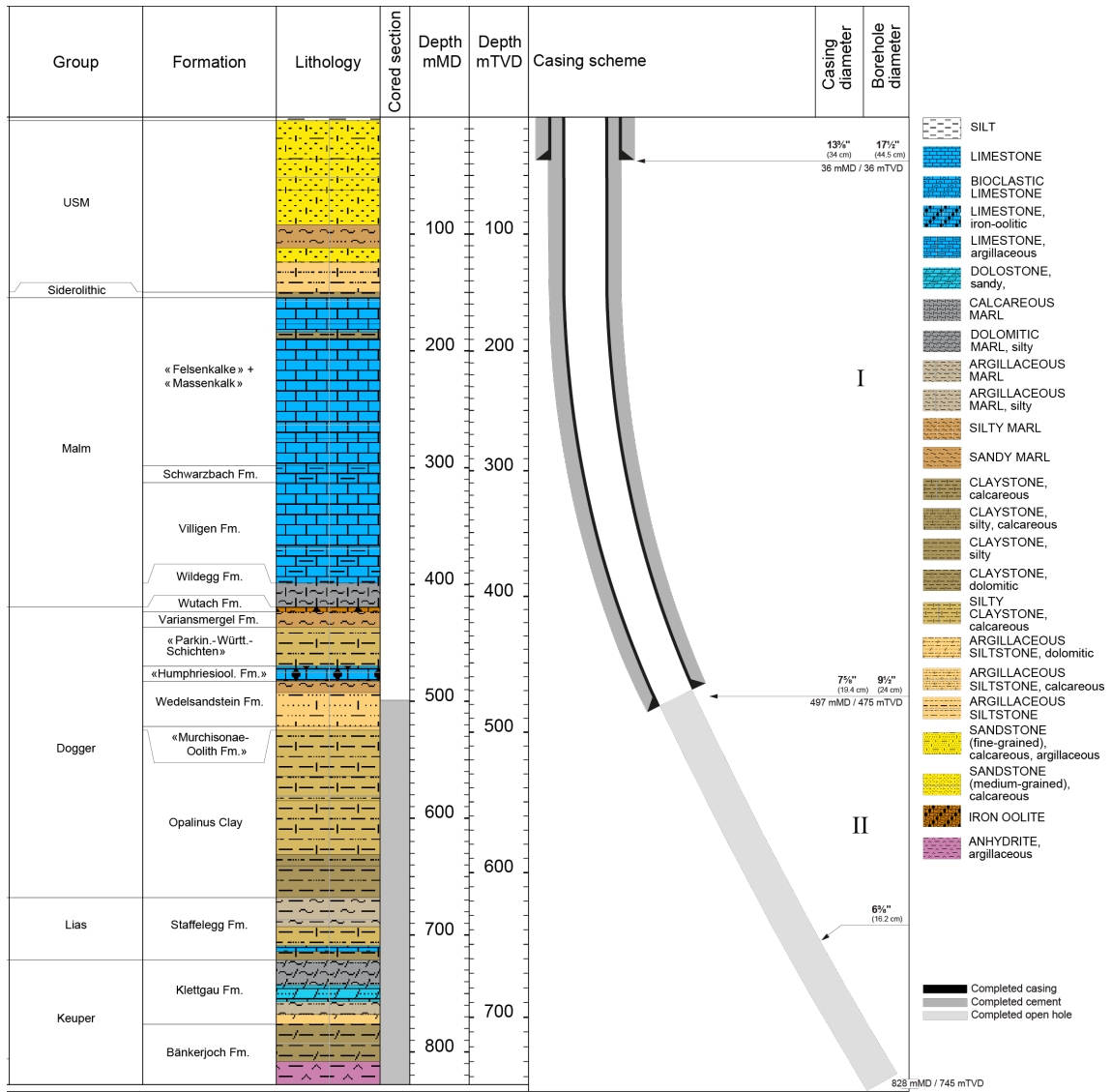
Fig. 1-6:   Lithostratigraphic profile and casing scheme for the RHE1-1 borehole[3]

1.3   Documentation structure for the RHE1-1 borehole

NAB 22-03 documents the majority of the investigations carried out in the RHE1-1 borehole, including laboratory investigations on core material. The NAB comprises a series of stand-alone dossiers addressing individual topics and a final dossier with a summary composite plot (Tab. 1-2).

This documentation aims at early publication of the data collected in the RHE1-1 borehole. It includes most of the data available approximately one year after completion of the borehole. Some analyses are still ongoing (e.g. diffusion experiments, analysis of veins, hydrochemical interpretation of water samples) and results will be published in separate reports.

The current borehole report will provide an important basis for the integration of datasets from different boreholes. The integration and interpretation of the results in the wider geological context will be documented later in separate geoscientific reports.

Tab. 1-2:   List of dossiers included in NAB 22-03

           Black indicates the dossier at hand.

Dossier	Title	Authors
I	TBO Rheinau-1-1: Drilling	M. Ammen & P.-J. Palten
II	TBO Rheinau-1-1: Core Photography	D. Kaehr & M. Gysi
III	TBO Rheinau-1-1: Lithostratigraphy	M. Schwarz, P. Schürch, P. Jordan, H. Naef, R. Felber, T. Ibele & F. Casanova
IV	TBO Rheinau-1-1: Microfacies, Bio- and Chemostratigraphic Analysis	S. Wohlwend, H.R. Bläsi, S. Feist-Burkhardt, B. Hostettler, U. Menkveld-Gfeller, V. Dietze & G. Deplazes
V	TBO Rheinau-1-1: Structural Geology	A. Ebert, S. Cioldi, E. Hägerstedt, L. Gregorczyk & F. Casanova
VI	TBO Rheinau-1-1: Wireline Logging and Micro-hydraulic Fracturing	J. Gonus, E. Bailey, J. Desroches & R. Garrard
VII	TBO Rheinau-1-1: Hydraulic Packer Testing	R. Schwarz, M. Willmann, P. Schulte, H. Fisch, S. Reinhardt, L. Schlickenrieder, M. Voß & A. Pechstein
VIII	TBO Rheinau-1-1: Rock Properties and Natural Tracer Profiles	J. Iannotta, F. Eichinger, L. Aschwanden & D. Traber
IX	*NAB 22-03 does not include a Dossier IX, as no rock-mechanical and geomechanical laboratory tests were conducted.*	
X	TBO Rheinau-1-1: Petrophysical Log Analysis	S. Marnat & J.K. Becker
	TBO Rheinau-1-1: Summary Plot	Nagra

1.4 Scope and objectives of this dossier

The dossier at hand complements the lithostratigraphic report (Dossier III) on the RHE1-1 borehole between the upper part of the Opalinus Clay and the top of the cored interval within the Wedelsandstein Formation (mainly from 561.26 m to – 499.12 m). The report documents data on microfacies analysis, ammonite- and palynostratigraphy as well as detailed geochemical (C, O and N isotopes) analyses. Preliminary results of these analyses already existed at data-freeze (07.01.2022), two months after the end of drilling operations and were integrated into the lithostratigraphic discussion and lithostratigraphic boundary definition (Dossier III).

The objectives of this report focusing on the upper part of the Opalinus Clay and its upper confining units are:

- to specify the macroscopic description by a few detailed microfacies analyses (components, matrix, cements),

- to allow a microfacies comparison of specific horizons, for example hardgrounds of the upper Opalinus Clay,

- to provide additional data on the diagenetic history of the sediment,

- to recover macrofossils from the stratigraphic interval of investigation which are significant for facies changes and chronostratigraphic data,

- to compile an additional independent dataset of palynomorphs for chronostratigraphic data,

- to provide detailed geochemical (C, O and N isotopes) analyses with one metre spacing from the stratigraphic interval of interest,

- to allow a chemostratigraphic correlation (stable isotopes) with other deep boreholes in the three siting regions,

- to support the definition of the lithostratigraphic units.

The detailed stratigraphy of the specific interval of the RHE1-1 borehole with core depth in metres can be found in Fig. 1-7. The stratigraphic intervals of interest for the different investigations (microfacies analysis, ammonite- and palynostratigraphy and geochemical analyses) and their specific sampling intervals are visualised in Fig. 1-8 with respect to the 1:5'000 lithostratigraphic profile.

All depths labelled with metres [m] in this report refer to "m MD core depth" if not stated otherwise.

TBO RHEINAU-1-1				
System / Period	**Group**	**Formation**	**Metres MD**	**Member / Sub-unit**
Quaternary			3	
Paleogene / Neogene	USM		149.9	
	Siderolithic		154.4	
Jurassic — Late — Malm	Malm	«Felsenkalke» + «Massenkalk»	298.1	
		Schwarzbach Fm.	312.7	
		Villigen Fm.	398.8	
		Wildegg Fm.	418.3	Effingen Mb.
			419.2	Birmenstorf Mb. and «Glaukonitsandmergel Bed»
Jurassic — Middle — Dogger	Dogger	Wutach Fm.	423.4	
		Variansmergel Fm.	436.6	
		«Parkinsoni-Württembergica-Sch.»	469.8	
		«Humphriesioolith Fm.»	474.9 / 481.8	
		Wedelsandstein Fm.	482.8	
		«Murchisonae-Oolith Fm.»	521.43	
		Opalinus Clay	524.61	«Sub-unit with silty calcareous beds»
			564.30	«Upper silty sub-unit»
			584.91	«Mixed clay-silt-carbonate sub-unit»
			640.86	«Clay-rich sub-unit»
			668.07	
Jurassic — Early — Lias	Lias	Staffelegg Fm.	675.84	Gross Wolf Mb.
			687.81	Rietheim Mb.
			691.63	Breitenmatt Mb. and Rickenbach Mb.
			692.89	Grünschholz Mb.
			709.21	Frick Mb.
			714.15	Beggingen Mb.
			721.46	Schambelen Mb.
Triassic — Late — Keuper	Keuper	Klettgau Fm.	743.34	Gruhalde Mb.
			757.16	Seebi Mb.
			765.67	Gruhalde Mb.
			767.79	Gansingen Mb.
			776.42	Ergolz Mb.
Triassic — ?806 M.		Bänkerjoch Fm.	808.28	«Claystone with anhydrite nodules»
				«Cyclic sequence»
			827.99	Final depth

Fig. 1-7: Rheinau-1-1 stratigraphy with core depth in metres [m MD]

Note that the RHE1-1 borehole is unique as it is not vertical but deviated and therefore, the measured depths (MD) are not the same as the true vertical depths (TVD). This leads to the fact that the thicknesses in the RHE1-1 well (MD) deviate from the surrounding ones (e.g. MAR1-1). A calculation from MD to TVD can be found in Dossier III of this report.
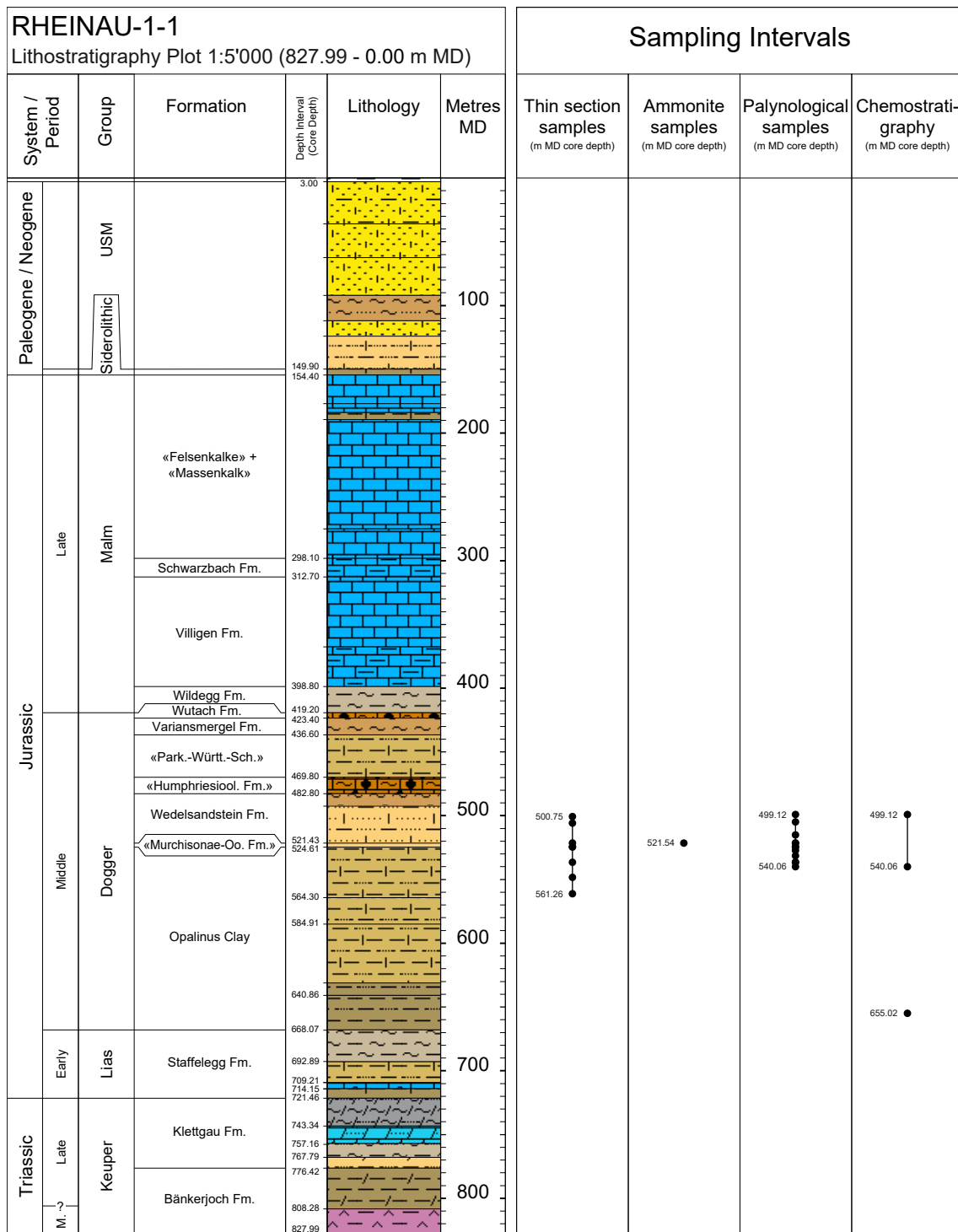
Fig. 1-8:   Lithostratigraphy plot (1:5'000) from the Mesozoic succession with the individual
            sampling intervals for thin sections, macrofossils, palynological analysis and chemo-
            stratigraphy

            1:5'000 stratigraphic plot modified from Dossier III.

2 Methods

2.1 Microfacies

Thin section preparation

All eight thin sections (TS) were cut edgewise from the core so that the long side is parallel to the coring direction and therefore covers as much of the stratigraphy as possible. The mean depth of the thin section corresponds to the Sample ID. Therefore, thin sections containing lithological boundaries may have Sample IDs that fall into only one of the two described intervals. However, the lower or upper range on the thin section still covers the interval. A list of all thin sections with their sampling range and Sample ID can be found in Appendix A1 of this report.

The eight thin sections are all from calcareous lithologies with a standard length of 4 cm and were prepared at the University of Basel. For better identification of the carbonate minerals calcite, Fe-calcite and Fe-dolomite, the left half of the thin sections was stained applying the technique of Dickson (1965). Thin sections with a macroscopic porosity were impregnated during preparation using a blue coloured epoxy resin to estimate the percentage of their porosity.

Thin section analyses

The thin sections were analysed using a Zeiss polarisation microscope. First, all allochemical components, biogenic particles, siliciclastics, matrix and diagenetic alterations as neomorphic minerals, cements and replacements were studied. Then, to obtain the percentage of the components etc., 100 points were counted with a net micrometre ocular. For detrital quartz-bearing thin sections, the average grain size was evaluated in millimetres. To count inhomogeneous sediments, two different sections were looked at and averaged. A selection of six thin section photographs for microfacies analysis is documented in Appendix B (Figs. B-1 to B-6).

Components, matrix and cements (definitions)

To describe thin sections, several allochemical components (described below) were counted, and their numbers are documented in Section 3.1 ('Microfacies'). Some of the specific terms used for the components or matrix are explained as follows:

Clay matrix, micrite, microsparite (or pseudosparite): Sedimented mud consisting of clay minerals, other very small silicate grains, heavy minerals (i.e. clay matrix) and/or microcrystalline carbonate ooze (i.e. micrite). Microsparite is defined as a mosaic of small calcite crystals formed by aggrading neomorphism; originally, it was micrite and not a diagenetic pore-filling cement. Alternatively, microsparite could also be the product of dedolomitisation as seen in the «Felsenkalke» and «Massenkalk».

Dolomitic matrix: primary microcrystalline dolostone ooze.

Limonitic matrix: Calcite micrite mixed with microcrystalline limonitic grains grown during diagenesis.

Limonitic echinoderms, limonitic bivalves: Fragments, parts of echinoderms and bivalves, with limonite filling the skeletal structure of the fossil.

Pellets, peloids, aggregates: the column of pellets also contains aggregates (lumps); that means "carbonate grains of various kinds are clumped together to form compound grains" (Bathurst 1975).

Fe-stromatolites and stromatolitic clasts: Iron-mineralised microbial mats and/or microbial clasts.

Fe-ooids or iron-ooids: Limonitic/goethitic or chamositic ooids, with a visible concentric structure; some iron-ooids are replaced by calcite (calcitic iron-ooids), a few of them show relicts of iron mineral layers (see RHE1-1-548.41, Fig. B-2, Appendix B).

Intraclasts: Rock fragments of early diagenetic cemented sediment, reworked and sedimented in the same sedimentary environment.

Calcite cement (sparite): "Normal" cement, calcite crystals grown – filled in – within the primary pore space or in leached components. In this column, the amount of calcite crystal pseudomorphs after gypsum was noted.

"Stellate cement": Calcite "cement" grown within the matrix and not filling primary or secondary pore space. The calcite crystals form small "stellates", i.e. a habitus typical for "hiatus beds" (firm-, hardgrounds; Wetzel & Allia 2000) or "hiatus concretions" (Voigt 1968).

Cone-in-cone calcite: Rows of piled calcite cones grown during diagenesis which were named "Tutenmergel" in the Swabian realm.

(Fe)-Dolomite: Normally dolomite rhombohedrons that originated during diagenesis; in special cases, the dolomite replaces gypsum crystals that were sedimented as detrital gypsum crystals. In some cases, the rhombohedrons consist of iron-dolomite, which are stained blue after the thin section staining.

Dedolomite: Calcite replacement of dolomite: each single dolomite rhombohedron is replaced by a few smaller calcite crystals. When it was a total dolostone and the calcitic replacement has been completed, the result is a thoroughly crystalline, sparitic/microsparitic limestone. In addition, another dedolomite type exists with larger calcite crystals jointly replacing a few dolomite crystals, thus forming a calcite mosaic similar to marble.

Anhydrite: Present in various forms: as a rock-forming mineral, as a vein mineral, mainly replacing "Fasergips", and as cement in sandstones (e.g. Ergolz Member of the Klettgau Formation).

Quartz cement: Authigenic quartz rims grown during diagenesis around detrital quartz grains; quartz/chalcedony in silicified bivalves (MAR1-1-569.18; Wohlwend et al. 2021b).

Porosity: Thin sections with a macroscopic porosity were impregnated during preparation using a blue coloured epoxy resin to estimate the volume percentage (vol.-%) of their porosity.

Hardground: Thin sections from hardgrounds document synsedimentarily cemented and lithified carbonate layers which have been exposed on the seafloor. During that time period, the hardgrounds are therefore mostly encrusted and bored by organisms and may consist of early marine calcite cements and are in parts mineralised by iron and manganese oxides or calcium phosphates.

2.2   Ammonite preparation

The cores from the upper part of the Opalinus Clay to the top of the cored interval within the Wedelsandstein Formation in RHE1-1 were carefully examined for macrofossils at the Würenlingen (Canton Aargau) core storage facility. The cores were examined for ammonites and other macrofossils on the bedding and fractured surfaces as well as on the outer surface of the core; the core itself was not broken open. A list with the taken ammonite sample, with the sampling range and Sample ID can be found in Appendix A2 of this report. In addition to the sampled ammonite, other conspicuous fossils were identified to the extent possible and entered in the list (Appendix A3), even when they were not subsequently, or only occasionally, recovered. The ammonite was then secured from the core and brought to the Natural History Museum in Bern where it was prepared and documented and archived in the earth sciences collection.

For the preparation, mechanical methods were used such as air tools and fine sandblasting equipment as well as a chemical etching method using potassium hydroxide (KOH). Sodium hydrogen carbonate was mainly used as abrasive.

2.3   Palynological sample preparation and quantitative analysis

Palynological processing of the twelve rock samples was carried out by PLS Palynological Laboratory Services Ltd. (Holyhead, Anglesey, LL65 4RJ, UK). Processing follows the standard protocol using concentrated HCl and concentrated HF, followed by a short oxidation with HNO_3 and, if necessary, treatment with ultrasound (e.g. Wood et al. 1996). The residues are sieved at a mesh size of 15 μm. Residues are mounted on microscope slides and analysed using transmitted light microscopy. A list of all samples with their sampling range and Sample ID can be found in Appendix A4 of this report.

Two consecutive counts were carried out in the quantitative microscopic analysis. In a first count 200 grains of all palynomorphs were counted and the number of dinoflagellate cysts was noted (column 'DA *Dinocysts (count 1)*' in Appendix C1). In a consecutive second count, only dinoflagellate cysts were counted until a total of 100 dinoflagellate cysts was reached. The reminder of the slide was checked for additional, out of count species. Taxa recorded out of count are marked with a '+', questionably identified taxa are marked with a '?' in the range chart. Occurrences of fungal remains are recorded semi-quantitatively (R = Rare, O = Occasional, C = Common, A = Abundant, S = Superabundant).

Results are illustrated using the software package StrataBugs v2.1 (Appendices C1 and C2). Numerical age dates used for the Composite Standard and the Depth/Age plot are in line with those of the *Geologic Time Scale 2016* (Ogg et al. 2016). On the range chart (Appendix C1) several abbreviations are used (AC = Acritarchs, ALBO = Algae, *Botryococcus* and *Pediastrum*, ALPR = Algae, Prasinophytes, ALZY = Algae, Zygnematophyceae, DA = Dinocyst abundance, DC = Dinoflagellate cysts, FT = Foraminiferal test linings, FU = Fungi, MP = Miscellaneous palynomorphs, SP = Spores and pollen. Several dinoflagellate cyst taxa contain a question mark in the name, as for example in *Evansia*? *eschachensis*. The question mark after the genus name indicates uncertainty regarding the correct taxonomical assignment of the species to the genus.

2.4   Chemostratigraphy

The sampling of the RHE1-1 borehole focused on the transition from the upper Opalinus Clay into the Wedelsandstein Formation (Dogger Group from 540.06 m to 499.12 m) and therefore primarily on clay mineral-rich layers. The sampling resolution was one metre, except for some intervals with denser sampling density (mainly hardgrounds and condensed intervals). All

57 samples were drilled with a micro-drill. In general, clay mineral-rich lithologies were sampled. Diagenetic calcite and siderite veins and nodules were avoided. The drilled powder amounted to around 1 g of material. A list of specific samples (n = 10) with results mainly from calcareous beds, calcareous concretions and septarian nodules can be found in Appendix D1 of this report.

Inorganic (carbonate) analyses

56 samples were analysed for **stable carbon** ($\delta^{13}C_{carb}$) and **oxygen isotope** ($\delta^{18}O_{carb}$) of bulk carbonate, 46 continuous samples (roughly in metre resolution) and additional 10 samples from specific calcareous beds and concretions in the Opalinus Clay (Appendix D1). Varying amounts of powder to reach approximately 120 μg of carbonate in the vial were weighed using a Mettler Toledo MT5 Fact microbalance in 12 ml vacutainers. The headspace was flushed with pure He, and then the samples were reacted with 100% phosphoric acid at 72 °C in a ThermoFisher GasBench II carbonate device connected to a ThermoFisher Delta V PLUS mass spectrometer. The instrument is calibrated with international carbonate standards NBS19 and NBS18 distributed by the International Atomic Energy Agency (IAEA), Vienna and internal standards (MS2 "Carrara marble"; $\delta^{13}C_{carb}$ = 2.16 ‰, $\delta^{18}O_{carb}$ = -1.85 ‰). The reproducibility of the measurements based on replicated standards was ± 0.05 ‰ for $\delta^{13}C_{carb}$ and ± 0.06 ‰ for $\delta^{18}O_{carb}$. All isotope measurements were performed at the Stable Isotope Laboratory of the ETH Zurich (Geological Institute). The isotope values are reported in the conventional delta notation with respect to the Vienna Pee Dee Belemnite (VPDB).

The **Total Carbonate content** (TCarb) was calculated based on a calibration using extracted CO_2 from the known weight of the internal standard material (MS2), which is composed to 100% of carbonate (calcite). The mean area of the m/z 44 peak (corresponding to the most abundant isotopologue $^{12}C^{16}O_2$) in the mass spectrometer allows the carbonate content to be estimated from the individual bulk rock samples. The individual uncertainty for TCarb represents the average from all standard deviations from the MS2 and is ± 7.70%. However, the TCarb values, calculated from the reaction of the phosphoric acid with the bulk rock, only reflect the carbonate that was able to react during the reaction time (~ 60 min). However, ankerite and especially siderite, for example, roughly require 60 h reaction time for full dissolution at 70 °C (Fernandez et al. 2016). Therefore, the calculated carbonate content (TCarb) does not completely represent the total amount of all different carbonates. The data reflect a mixed signal composed mostly of calcite and dolomite with a smaller component of the other more resistant carbonates (see also Wohlwend et al. 2019).

Organic analyses

The powders remaining after inorganic analysis from 47 samples were decarbonated in quantities of less than 1 g in 10 ml of 3 M HCl for 12 h in 15 ml centrifuge tubes, to ensure the complete removal of carbonate. For neutralisation purposes, the residue was subsequently washed three times with deionised water, and then centrifuged and decanted. After drying at 70 °C in an oven for at least 72 h, the samples were homogenised with a mortar and pestle. Depending on the organic carbon content of each specific sample, a different amount was weighed in a tin capsule using a Mettler Toledo MT5 Fact microbalance, so that approximately the same amount of organic carbon was always measured.

$\delta^{13}C_{org}$ and $\delta^{15}N_{org}$ were measured by flash combustion on a ThermoFisher Scientific FlashEA elemental analyser connected to a Delta V isotope ratio mass spectrometer (IRMS) operated in continuous flow mode. The samples were combusted in an O_2 atmosphere in a quartz reactor at 1'020 °C packed with $(Co_3O_4)Ag$ and Cr_2O_3 to form CO_2, N_2, NO_X and H_2O. These gases were then transferred through a reduction reactor containing elemental Cu at 600 °C to remove excess

O_2 and to reduce NO_X to N_2. H_2O and SO_X were subsequently removed using anhydrous $Mg(ClO_4)_2$ and elemental Ag. Then, N_2 and CO_2 were separated in a packed gas chromatographic column and analysed for their isotopic composition using the IRMS. Isotope ratios are reported in conventional delta notation with respect to atmospheric N_2 (AIR) and VPDB standards, respectively. The methods were calibrated with the International Atomic Energy Agency (IAEA)-N1 ($\delta^{15}N$ = 0.45 ‰), IAEA-N2 ($\delta^{15}N$ = +20.41 ‰) and IAEA-N3 ($\delta^{15}N$ = +4.72 ‰) reference materials for nitrogen, and NBS22 ($\delta^{13}C$ = -30.03 ‰) and IAEA-CH-6 ($\delta^{13}C$ = -10.46 ‰) for carbon. Reproducibility of the measurements is better than ± 0.2 ‰ for both nitrogen and carbon. Reproducibility and accuracy of the measurements are based on replicate analyses of the internal laboratory standards atropine, peptone and nicotinamide. All geochemical measurements were performed at the Stable Isotope Laboratory of the ETH Zurich (Geological Institute).

The **Total Organic Carbon** (TOC_{decarb}) and **Total Nitrogen** (TN_{decarb}) contents of the decarbonised samples were calculated based on the known carbon and nitrogen contents of atropine (70.56 wt.-% C, 4.84 wt.-% N). The individual uncertainty for TOC_{decarb} represents the average from all standard deviations from atropine during that calculation and is ± 0.40%, respectively ± 0.06% for the TN_{decarb}. The calculated TN_{decarb} reflects a mixture of bound inorganic and organic nitrogen and therefore also contains ammonium, which substitutes for K^+ in the interlayer exchange sites of illite (Scheffer & Schachtschnabel 1984).

The **Carbon-to-Nitrogen ratio** (C/N ratio) is a ratio of the mass of carbon to the mass of nitrogen. In this study, the ratio was calculated using the TOC_{decarb} and the TN_{decarb}. As mentioned above, the C/N ratios can also be influenced by inorganic nitrogen in the form of soil-derived ammonium (Scheffer & Schachtschnabel 1984). Due to this inorganic nitrogen, the C/N ratios of sediments containing additional inorganic nitrogen will decrease. Therefore, C/N ratios are referred to as organic carbon/total nitrogen (TOC_{decarb}/TN_{decarb}) giving the ratio of the C and N masses of the decarbonised samples (C_{org}/N_{org}). The calculated ratios allow to distinguish between marine (C/N ≤ 10; Parsons 1975) *versus* terrigenous matter (C/N ≥ 12; Kukal 1971) in marine sediments.

$$\frac{C_{org}}{N_{org}} = \frac{TOC_{decarb}}{TN_{decarb}} * \frac{atomic\ mass\ (C)}{atomic\ mass\ (N)} = \frac{TOC_{decarb}}{TN_{decarb}} * \frac{14.007}{12.011}$$

The **Total Organic Carbon** (TOC) of the whole/bulk sample was calculated using the semi-quantitative carbonate content (TCarb) and semi-quantitative TOC_{decarb} content based on the following equation:

$$TOC = (1 - TCarb) * TOC_{decarb}$$

3   Results

3.1   Microfacies

Opalinus Clay (RHE1-1-561.26, 548.41, 536.60)

All three thin sections, RHE1-1-561.26, 548.41 and 536.60, come from calcareous "hiatus beds" or hardgrounds, intercalated mainly in the silty claystone succession. The basis for each of these three beds are biogenic components – echinoderm skeletal elements and bivalves – then intraclasts, nodules and in one case iron-ooids (RHE1-1-548.41).

Thin section RHE1-1-561.26 consists of echinoderms (9 vol.-%; see Tab. 3-1 for all vol.-% data in this section), bivalves (11 vol.-%), intraclasts (40 vol.-%), quartz silt to fine-sand (4 vol.-%) and pyrite (7 vol.-%) (Fig. B-1; see Appendix B for all figures in this section). A lot of pyrite is also enclosed in bivalves and intraclasts, but these pyrites are part of the bivalves and the intraclasts. The components are embedded in clay matrix (11 vol.-%) with "stellate cement" (11 vol.-%) and siderite (7 vol.-%).

The bed of RHE1-1-548.41 is a multi-layered hardground: the thin section contains calcitic iron-ooids (iron minerals are replaced by calcite; 10 vol.-%), intraclasts (7 vol.-%), then echinoderms (12 vol.-%) and bivalves (21 vol.-%) (Fig. B-2), as well as some quartz (8 vol.-%) and pyrite (4 vol.-%) in a sideritic, marly matrix (8 and 30 vol.-%). The here mentioned calcitic iron-ooids have been noted in the "Fe-ooids" column in Tab. 3-1 with an asterisk behind the number.

Micritic nodules (60 vol.-%) dominate the thin section sample RHE1-1-536.60 (Fig. B-3). Echinoderm skeletal elements (17 vol.-%), marly matrix (12 vol.-%) and siderite (11 vol.-%) make the other part.

«Murchisonae-Oolith Formation» (RHE1-1-524.57, 524.52, 521.47)

From the thin hardground at the base of the «Murchisonae-Oolith Formation» (524.61 – 524.51 m) the two thin sections RHE1-1-524.57 and 524.52 were taken: the lower one represents the lithology of the bed, the second one is used for the analysis of an unknown calcite crust underneath an intraclast. The third thin section (RHE1-1-521.47 derives from the hardground at the top of the formation (condensed bed from 521.50 – 521.43 m).

RHE1-1-524.57 represents the lithology of the lower hardground and contains 42 vol.-% iron-ooids and is therefore referred to as an iron-oolite. However, most of the iron-ooids are replaced by calcite and are therefore also marked by an asterisk in Tab. 3-1, but many have retained their ferruginous or limonitic core (Fig. B-4). Echinoderms (8 vol.-%), bivalves (6 vol.-%), intraclasts (5 vol.-%), pyrite (12 vol.-%) and micrite matrix (27 vol.-%) complete the composition.

RHE1-1-524.52 shows two parts: a micritic intraclast (79 vol.-%) and a calcitic biogenic crust (21 vol.-%). The intraclast consists of 7 vol.-% (referred on 100% counted thin section area) echinoderms, 4 vol.-% bivalves, 10 vol.-% quartz sand, 5 vol.-% pyrite and 53 vol.-% micrite matrix. The biogenic crust has an irregular cellular structure (Fig. B-5) of an encrusting organism.

The thin section RHE1-1-521.47, from the upper hardground at the top of the «Murchisonae-Oolith Formation», consists of an iron-oolitic, bioclastic limestone and a sandy, microsparitic limestone. The microfacies analysis only concern the layer with iron-ooids, consisting of echinoderms (16 vol.-%), bivalves (15 vol.-%), other biogenes, e.g. bryozoans (2 vol.-%), iron-ooids (13 vol.-%), quartz sand (4 vol.-%), micrite matrix (45 vol.-%) and pyrite (5 vol.-%). The iron-ooids are for the most part replaced by calcite (Fig. B-6) and are therefore also marked by an asterisk in Tab. 3-1.

Wedelsandstein Formation (RHE1-1-505.88 and 500.75)

The two thin sections RHE1-1-505.88 and RHE1-1-500.75 were taken from sandy, bioclastic limestone beds, which are located within the argillaceous sandstone succession of the Wedelsandstein Formation.

Both samples, RHE1-1-505.88 and RHE1-1-500.75, have a very similar composition: sponge spicules (11, resp. 14 vol.-%), bivalves (11, resp. 10 vol.-%), other biogenes, including serpulids (1, resp. 2 vol.-%), pellets and peloids (12, resp. 10 vol.-%), quartz sand (29, resp. 26 vol.-%), micas (2 vol.-%) and microsparitic matrix, incl. little limonitic matrix (27, resp. 22 vol.-%), as well as few pyrite (3 vol.-%) and limonitic nodules (RHE1-1-500.75: 4 vol.-%).

Tab. 3-1: Microfacies analysis from RHE1-1 (561.26 – 500.75 m; numbers in vol.-%)

Microfacies analysis RHE1-1 (561.26 - 500.75 m)	clay matrix, micrite, microsparite	dolomitic matrix	limonitic matrix	echinoderms	bivalves	limonitic echinod. + bivalves	serpulids	corals	sponges, spicules	other biogenes	Fe-stromatolite + stromatolitic clasts	pellets, peloids, aggregates	ooids	oncoids	Fe-ooids	intraclasts, nodules	detrital quartz + silic. rock fragm.	quartz grainsize (mm)	calcite cement	"stellate cement" (s) cone-in-cone calcite (c)	(Fe-)dolomite	dedolomite	anhydrite, gypsum	quartz cement	pyrite	limonite, Fe-min. nodules	siderite	glauconite	mica	porosity
500.75m: bioclastic limestone (sandy) *Wedelsandstein Fm.*	18		4	5	10		2		14	2		10					26	0.08							3	4			2	
505.88m: bioclastic limestone (sandy) *Wedelsandstein Fm.*	27			4	11				11	1		12					29	0.07							3				2	
521.47m: biocl. limestone (Fe-oolitic) *«Murchisonae-Oolith Fm.»*	45			16	15					2					13*		4	0.09							5					
524.52m: intraclast with biogenic crust *«Murchisonae-Oolith Fm.»*	53			7	4					21							10	0.10							5					
524.57m: iron-oolite, calcareous *«Murchisonae-Oolith Fm.»*	27			8	6										42*	5									12					
536.60m: biocl. cal. marl + micr. nodules *Opalinus Clay*	12			17												60											11			
548.41m: biocl. cal. marl with Fe-ooids *Opalinus Clay*	30			12	21										10*	7	8	0.06							4		8			
561.26m: biocl. cal. marl + micr. nodules *Opalinus Clay*	11			9	11											40	4	0.06		11					7		7			

3.2   Ammonite stratigraphy

Due to the short examination section at RHE1-1 only one ammonite specimen was recovered (depth 521.54 m). The ammonite was not documented with a photograph.

In general, the more ammonites are present in a specific profile section, the more precisely the biostratigraphic classification of that section can be determined (Tab. 3-2). Furthermore, it must be considered that not all ammonites have the same index value and that the state of preservation of the objects also plays an important role in the biostratigraphic determination. Therefore, a certain error must always be expected. This error is in the range of about one ammonite Subzone (SZ) but can be as high as one ammonite Zone (Z) when the available data is insufficient.

«Murchisonae-Oolith Formation»

521.54 m: Ammonite. Graphoceratidae indet. Truncated specimen with a poor preservation. Age: probably Late Aalenian to earliest Bajocian, probably Concavum Zone to earliest Discites Zone. Lithology: Grey iron-oolitic limestone (argillaceous) with grey sandy lithoclasts. Other fossils: Bivalves and echinoderm ossicles.

Tab. 3-2:   Ammonite and other macrofossil determination from RHE1-1

Depth [m MD]	Identification	Ammonite Zone (Subzone) or Age
521.54	Graphoceratidae indet.	probably Concavum Zone to earliest Discites Zone

Left table

System	Stage		Zone	Subzone
Jurassic	Oxfordian	Late	Bifurcatus	Grossouvrei
				Stenocycloides
		Middle	Transversarium	Rotoides
				Schilli
				Luciaeformis
				Parandieri
			Plicatilis	Antecedens
				Vertebrale
		Early	Cordatum	Cordatum
				Costicardia
				Bukowski
			Mariae	Praecordatum
				Scarburgense
	Callovian	Late	Lamberti	Lamberti
				Henrici
			Athleta	Spinosum
				Proniae
				Phaeinum
		Middle	Coronatum	Grossouvrei
				Obductum
			Jason	Jason
				Medea
			Calloviense	Enodatum
				Calloviense
		Early	Koenigi	Galilaeii
				Curtilobus
				Gowerianus
			Herveyi	Kamptus
				Terebratus
				Keppleri
	Bathonian	Late	Discus	Discus
				Hollandi
			Orbis	Hannoveranus
				Blanazense
		Middle	Hodsoni	
			Morrisi	
			Subcontractus	
			Progracilis	
		Early	Zigzag	Tenuiplicatus
				Yeovilensis
				Macrescens
				Convergens
	Bajocian	Late	Parkinsoni	Bomfordi
				Truellei
				Acris
			Garantiana	Tetragona
				Garantiana
				Dichotoma
			Niortense	Baculata
				Polygyralis
				Banksii
		Early	Humphriesianum	Blagdeni
				Humphriesianum
				Romani
				Pinguis
			Sauzei	Macrum
				Kumaterum
			Laeviuscula	Laeviuscula
				Trigonalis
			Ovale	
			Discites [?]	
	Aalenian	Late	Concavum [?]	Formosum
				Concavum
		Middle	Bradfordensis	Gigantea
				Bradfordensis
			Murchisonae	Murchisonae
				Haugi
		Early	Opalinum	Bifidatum *
				Opalinum

Right table

System	Stage		Zone	Subzone
Jurassic	Toarcian	Late	Aalensis	Torulosum
				Aalensis
			Levesquei	Moorei
				Levesquei
			Insigne	Dispansum
				Insigne
			Thouarsense	Fallaciosum
				Thouarsense
			Variabilis	
		Early	Bifrons	Crassum
				Fibulatum
				Commune
			Falcifer	Falcifer
				Elegans
				Exaratum
				Elegantulum
			Tenuicostatum	Semicelatum
				Clevelandicum
				Paltum
	Pliensbachian	Late	Spinatum	Hawskerense
				Apyrenum
			Margaritatus	Gibbosus
				Subnodosus
				Stokesi
		Early	Davoei	Figulinum
				Capricornus
				Maculatum
			Ibex	Luridum
				Valdani
				Masseanum
			Jamesoni	Jamesoni
				Brevispina
				Polymorphus
				Taylori
	Sinemurian	Late	Raricostatum	Aplanatum
				Macdonnelli
				Raricostatum
				Densinodulum
			Oxynotum	Oxynotum
				Simpsoni
			Obtusum	Denotatus
				Stellare
				Obtusum
			Turneri	Turneri
		Early	Semicostatum	Sauzeanum
				Scipionanum
				Charlesi
			Bucklandi	Bucklandi
				Rotiforme
				Conybeari
	Hettangian		Angulata	Complanata
				Extranodosa
			Liasicus	Laquaeus
				Portlocki
			Planorbis	Johnstoni
				Planorbis

RHE1-1

Grey highlighted zones and subzones are documented in the drill core with ammonites. Fields with additional interrogation points are not surely proven with ammonites.

Biostratigraphy modified after Cariou & Hanzpergue (1997)
* after Dietze et al. (2021), former «Comptum» Subzone

Fig. 3-1:   Zones which are probably documented by the ammonite in RHE1-1

3.3 Palynostratigraphy

The 12 studied samples yielded mostly a good palynological residue with rich and diverse palynofloras. Preservation is good. The palynomorph assemblages are mainly composed of dinoflagellate cysts and pollen and spores. Minor components are prasinophytes, acritarchs, foraminiferal test linings and green algae (e.g. *Botryococcus*). A total of 59 dinoflagellate cyst taxa, 17 other aquatic palynomorphs and 46 pollen and spore taxa are recorded.

Some reworked sporomorphs (*Densosporites* spp.) indicate erosion of Triassic sediments in the source area. Other reworking is indicated by the occurrence of a few single specimens of the dinoflagellate cyst *Luehndea spinosa*, a typical Early Jurassic species with a main distribution in the Late Pliensbachian and earliest Toarcian.

The studied samples from the RHE1-1 core are dated to span the interval from the Aalenian to the Early Bajocian. There are 5 sample intervals differentiated and, where possible, assigned to ammonite biostratigraphy. A list of the analysed samples and the age dating of each sample is given in Tab. 3-3. The indicated ages, zones (Z) and subzones (SZ) for each sample are the result of the palynostratigraphical analysis and interpretation. The results of the quantitative analysis are illustrated in a Range Chart (Appendix C1). A Depth/Age plot is illustrated in Appendix C2.

Sample interval 540.06 – 536.73 m (2 samples): Early Aalenian, Opalinum Zone, Opalinum Subzone

Dinoflagellate cyst assemblages of this sample interval are moderately rich and diverse. They are composed of common *Evansia*? cf. *granochagrinata*, representatives of the families Phallocystaceae (*Dodekovia* spp., *D. knertensis*, *D. pseudochytroeides*, *Ovalicysta hiata*, *Parvocysta*? *tricornuta*, *Phallocysta*? *frommernensis*, *Reutlingia nasuta*) and Valvaeodiniaceae (*Valvaeodinium* spp., *V. brevepellitum*, *V. sphaerechinatum*, *V. vermipellitum*), species of *Nannoceratopsis* (*Nannoceratopsis* spp., *N. dictyambonis*, *N. gracilis* s.s. and s.l., *N. plegas dictyornata*, *N. plegas plegas*, *N.* sp. B, *N. triangulata*) and *Scriniocassis* (*S. limbicavatus*, *S. priscus*, *S. weberi*) as well as *Hystrichodinium*? sp. in Feist-Burkhardt & Pross (2010), *Kallosphaeridium praussii* and *Mancodinium semitabulatum*.

The sample interval is defined by the occurrences of *Kallosphaeridium praussii*, *Phallocysta*? *frommernensis* and *Nannoceratopsis triangulata* to the last occurrence of *Phallocysta*? *frommernensis* at the top of the interval and the first occurrence of questionable *Batiacasphaera* sp. A in the sample interval above.

Feist-Burkhardt & Pross (2010) determined four marker species for the Early Aalenian Opalinuston Formation (Germany stratigraphy) that are *Kallosphaeridium praussii*, *Phallocysta*? *frommernensis, Nannoceratopsis triangulata* and *Wallodinium laganum*. Three of the four marker species occur in this interval. The genus *Batiacasphaera* has its FAD (First Appearance Datum) in the upper part of the Opalinum Zone with *Batiacasphaera* sp. A often being abundant in Bifidatum Subzone of the Opalinum Zone.

The sample interval is dated Early Aalenian Opalinum Zone, Opalinum Subzone.

Sample interval 536.42 – 524.82 m (4 samples): Early Aalenian, Opalinum Zone, probably Bifidatum Subzone

Assemblages in this interval are quite similar to below. The base of the interval is characterised by the first occurrence of questionable *Batiacasphaera* sp. A. Higher up in the interval *Batiacasphaera* spp. and *Batiacasphaera* sp. A become common. The genus *Nannoceratopsis* is

abundant and diverse, including all subspecies of *N. plegas* (*N. plegas brevicorna, N. plegas dictyornata, N. plegas plegas*) and the first occurrences of *Nannoceratopsis* sp. 1, sp. 2 and *N. triceras*. Unquestionable specimens of the marker species *N. triangulata* occur up to the top of the interval. *Scriniocassis limbicavatus, S. priscus* and *S. weberi* are present throughout. *Wallodinium laganum* occurs in the lower part of the interval.

The interval is defined from the first occurrence of questionable *Batiacasphaera* sp. A to its last common occurrence, the last occurrence of unquestionable *Nannoceratopsis triangulata* at the top of the interval and the first occurrence of questionable *Dissiliodinium* spp. at the base of the interval above.

The genus *Batiacasphaera* has its FAD in the upper part of the Opalinum Zone with *Batiacasphaera* sp. A often being abundant in the Bifidatum Subzone of Opalinum Zone. The LAD (Last Appearance Datum) of *Nannoceratopsis triangulata* is considered to be at the top of the Opalinum Zone. The FAD of *Dissiliodinium* spp. is within Bradfordensis Zone.

The interval is interpreted Opalinum Zone, probably Bifidatum Subzone.

The occurrence of *Luehndea spinosa* in all samples of the interval, as well as in the interval above, indicates reworking of Early Jurassic Late Pliensbachian to earliest Toarcian sediments in the source area.

Sample interval 524.27 – 521.79 m (2 samples): ?Early Aalenian, Opalinum Zone to ?Middle Aalenian, Bradfordensis Zone

Assemblages in this interval are still quite similar to below with i.a. some representatives of the families Phallocystaceae and Valvaeodiniaceae, abundant and diverse *Nannoceratopsis* including the subspecies of *N. plegas,* questionable *N. triangulata* and *N. triceras*, all species of *Scriniocassis* (*S. limbicavatus, S. priscus, S. weberi*), as well as *Batiacasphaera* spp., *Evansia*? cf. *granochagrinata*, *Kallosphaeridium praussii* and *Mancodinium semitabulatum*. In addition, there are the first occurrences of a few single specimens of questionable *Dissiliodinium* spp. and questionable *Evansia*? *spongogranulata*.

The interval is defined by the co-occurrence of questionable *Nannoceratopsis triangulata* and *Scriniocassis weberi* on the one hand and questionable *Dissiliodinium* spp. and questionable *Evansia*? *spongogranulata* on the other.

The LADs of *Nannoceratopsis triangulata* and *Scriniocassis weberi* are at the top of Opalinum Zone. The LADs of *Scriniocassis limbicavatus* and *S. priscus* are at the top of Bradfordensis Zone. The FAD of *Evansia*? *spongogranulata* is in the Murchisonae Zone and that of *Dissiliodinium* spp. is within the Bradfordensis Zone.

The co-occurrence of these species is unusual and points to either a natural mixture of assemblages of different age (Opalinum, Murchisonae and Bradfordensis zones) due to condensation or reworking, or may be due to contamination of the samples of Early Aalenian age with slightly younger material of the Middle Aalenian.

The interval is dated questionably Opalinum Zone to questionably Bradfordensis Zone.

The occurrence of *Luehndea spinosa* in all samples of the interval, as well as in the interval below, indicates reworking of Early Jurassic Late Pliensbachian to earliest Toarcian sediments in the source area.

Sample interval 521.37 – 504.95 m (3 samples): Early Bajocian, Ovale Zone

The dinoflagellate cyst assemblages in this interval differ a lot from the samples below. Representatives of the genus *Dissiliodinium* are abundant. There are numerous first occurrences at the base of the interval, i.a. *Dissiliodinium* aff. *giganteum*, *D. giganteum*, *D. lichenoides*, *Evansia*? *eschachensis*, *Gongylodinium erymnoteichon*, *Moesiodinium raileanui*, and further up in the interval, *Durotrigia* spp., *D. daveyi*, *Moesiodinium* sp. 2 and *Pareodinia* spp. The species *Dissiliodinium giganteum* is abundant and shows an acme from sample 515.13 m upwards. *Andreedinium elongatum* has its last occurrence in sample 521.37 m, and the rare species *Gresslyodinium mirabile* is recorded in the sample at 504.95 m.

The interval is defined by the first occurrence of *Dissiliodinium giganteum* to the first occurrence of *Cavatodissiliodinium hansgochtii* in the interval above.

The FAD of *Dissiliodinium giganteum* is in the Ovale Zone. The LAD of *Andreedinium elongatum* is also in the Ovale Zone. The FAD of *Cavatodissiliodinium hansgochtii* is in the Laeviuscula Zone.

The interval is dated Ovale Zone.

Sample 499.12 m (1 sample): Early Bajocian, Ovale to Laeviuscula Zone

In addition to species known from below, the sample shows the first occurrence of common *Cavatodissiliodinium hansgochtii*. *Evansia*? *eschachensis* is still present. *Batiacasphaera laevigata* is not recorded.

The interval is defined by the co-occurrence of *Evansia*? *eschachensis* and *Cavatodissiliodinium hansgochtii*.

The LAD of *Evansia*? *eschachensis* is in the Ovale Zone. The FADs of *Cavatodissiliodinium hansgochtii* and *Batiacasphaera laevigata* are in the Laeviuscula Zone.

The sample is dated Ovale to Laeviuscula Zone.

Tab. 3-3: List of analysed palynology samples from RHE1-1

The indicated ages, zones and subzones for each sample are the result of the palynostratigraphical analysis and interpretation.

Depth [m MD]	Age	Zone & Subzone
499.12	Early Bajocian	Laeviuscula – Ovale Zone
504.95	Early Bajocian	Ovale Zone
515.13	Early Bajocian	Ovale Zone
521.37	Early Bajocian	Ovale Zone
521.79	?Middle – ?Early Aalenian	?Bradfordensis – ?Opalinum Zone
524.27	?Middle – ?Early Aalenian	?Bradfordensis – ?Opalinum Zone
524.82	Early Aalenian	Opalinum Zone (probably Bifidatum SZ)
527.26	Early Aalenian	Opalinum Zone (probably Bifidatum SZ)
531.50	Early Aalenian	Opalinum Zone (probably Bifidatum SZ)
536.42	Early Aalenian	Opalinum Zone (probably Bifidatum SZ)
536.73	Early Aalenian	Opalinum Zone (Opalinum SZ)
540.06	Early Aalenian	Opalinum Zone (Opalinum SZ)

3.4 Chemostratigraphy

The sampling of the RHE1-1 cores focused primarily on the transition from the uppermost part of the Opalinus Clay to the lowermost part of the Wedelsandstein Formation (Figs. 3-2 and 3-3) and, therefore inter alia on clay mineral-rich intervals. The data presented here (applies for both subsequent figures in this section) is shown in comparison to other data collected during the drilling campaign: Stratigraphic profile after Dossier III and Dry Clay (values in wt.-%, vertical axis in m MD log depth; *cf.* Dossier X). In the two figures the formation boundaries were highlighted with black lines and the uppermost informal sub-unit boundary of the Opalinus Clay with a grey line. For the «Murchisonae-Oolith Formation» the following stratigraphic abbreviation was used in Figs. 3-2 and 3-3: «M.-O.».

In addition to the continuous samples (roughly in metre resolution), some specific samples were taken (Appendix D1) to complete the information about the calcareous beds. One sample (524.56 m) was drilled directly from the remaining thin section block to correlate the bulk geochemical data with the microfacies analysis. All these data points are distinguished in two different colours on Fig. 3-2 (in light blue: calcareous samples, such as firm- and hardgrounds or "hiatus beds"; in violet: septarian nodules) but may not be shown on the individual plots because of the data ranges (see Appendix D1 for data).

The data will be discussed in only one interval because of the rather limited interval of investigation: Dogger Group – mainly transition from Opalinus Clay to Wedelsandstein Formation. Not all data are discussed to the same extent as for example the $\delta^{18}O_{carb}$ and $\delta^{15}N_{org}$ data. The oxygen isotopes are strongly influenced by diagenesis. This can be exemplarily shown with the measured belemnites in the Lias Group in MAR1-1 (green points in Figure 3-2 in Wohlwend et al. 2021b). These are 3 to 4 ‰ more positive than the marlier bulk rock and therefore much less diagenetically overprinted. The nitrogen isotopes may not be as meaningful in some cases, because the combined $\delta^{13}C_{org}$ and $\delta^{15}N_{org}$ measurements showed a too low concentration of N in most of the measurements.

Although, the calculated carbonate content (TCarb) is only a semi-quantitative method, the values normally correspond quite good to the XRD values measured at the University of Bern (see other reports, e.g. MAR1-1: Wohlwend et al. 2021b). From the RHE1-1 cores no XRD data were collected and therefore no visual comparison can be shown. As discussed in Wohlwend et al. (2019) based on measurements from the BDB-1 borehole at the Mont Terri Rock Laboratory, the values calculated here follow nicely the calcite and dolomite wt.-% with an additional mixed signal from the other carbonates (mainly siderite). Because during the reaction time of 60 min at 72 °C, a complete reaction for example for siderite does not take place.

Dogger Group – mainly transition from Opalinus Clay to Wedelsandstein Formation

The interval described in the following section, the Dogger Group (the uppermost part of the Opalinus Clay, «Murchisonae-Oolith Formation» and the transition into the lower part of the Wedelsandstein Formation), is also the interval at the main focus of these investigations (Figs. 3-2 and 3-3).

The semi-quantitative carbonate content (TCarb) values from the uppermost informal sub-unit («Sub-unit with silty calcareous beds»: 564.30 – 524.61 m) document a slight increase from 540.06 m to the value at 532.00 m, which was analysed from a more calcareous bed (57 wt.-%). The average values below that calcareous marl bed (532.25 – 531.97 m) range between 12 and 15 wt.-% and are interrupted by two calcareous horizons. They are marked in Fig. 3-2 by

a thicker violet line and dot (septarian nodule at 539.20 m) and a bioclastic marl with micritic nodules (see thin section RHE1-1-536.60) marked by a light blue line and dot (see Appendix D1 for data). The blue measurement at 536.53 m was analysed from the bed between 536.64 m and 536.40 m. The TCarb values above that prominent calcareous marl bed (532.25 – 531.97 m) clearly show a slight shift to less calcareous value between 10 and 12 wt.-% until 526.90 m and then a drastic decrease to values only around 3 to 5 wt.-% just below the top of the Opalinus Clay. The lithological boundaries from the following «Murchisonae-Oolith Formation» are marked by three blue measurements, one from the basal hardground (524.56 m) and two from the top hardground (521.74 m and 521.50 m). The TCarb values between these calcareous beds are ranging between 7 and 11 wt.-%. The above following Wedelsandstein Formation, up to the top of the cored interval at 499.10 m (uppermost sample at 499.12 m), has a clearly higher average TCarb content which is between 15 and 25 wt.-% with two clearly more calcareous values (509.00 m and 499.12 m). The three additional blue measurements are representing some of the calcareous interbeds typical for the Wedelsandstein Formation in the siting region Zürich Nordost.

The $\delta^{13}C_{carb}$ data show at first glance a clear difference between the uppermost Opalinus Clay and the above following «Murchisonae-Oolith Formation» and Wedelsandstein Formation. The $\delta^{13}C_{carb}$ values from the Wedelsandstein Formation (uppermost sample at 499.12 m) are, with a few exceptions, always above 1 ‰. Whereas the values from the «Murchisonae-Oolith Formation» range around 0 ‰ to 1 ‰ in the uppermost part. The data from the Opalinus Clay have a clear wider and more negative range. Between the two above mentioned calcareous beds (536.64 – 536.40 m and 532.25 – 531.97 m) the $\delta^{13}C_{carb}$ data document somehow more negative values (-3.6 ‰ at 536.00 m). Above the upper calcareous bed, the $\delta^{13}C_{carb}$ data reach values up to -0.2 ‰ at 531.00 m which then decrease to the top of Opalinus Clay (-3.3 ‰ at 525.07 m).

The $\delta^{13}C_{carb}$ data from the septarian nodules document a clear early diagenetic signal (e.g. Wetzel & Allia 2000). The septarian nodules are the only macroscopic features with very negative $\delta^{13}C_{carb}$ values (-16.9 to -23.1 ‰, Appendix D1). However, very fine authigenic calcite was probably also precipitated in the very fine original porosity of the Opalinus Clay, which led to the more negative $\delta^{13}C_{carb}$ values in the upper more negative excursion bounded by the two calcareous beds (see also Wohlwend et al. 2016).

The $\delta^{13}C_{org}$ data (Fig. 3-3) show a somehow similar picture comparing the overall trends from the uppermost Opalinus Clay to the above following «Murchisonae-Oolith Formation» and Wedelsandstein Formation. The $\delta^{13}C_{org}$ values clearly are lower in the Opalinus Clay and higher in the above following two formations. The uppermost part of the Opalinus Clay from the «Sub-unit with silty calcareous beds» documents a positive $\delta^{13}C_{org}$ trend from -26.8 ‰ at the base (540.06 m) to an overall positive peak in the Opalinus Clay at 531.00 m with -26.2 ‰. This more positive $\delta^{13}C_{org}$ excursion is measured in the sample just above the uppermost calcareous bed, similar to the positive shift in the $\delta^{13}C_{carb}$ data. To the top of the Opalinus Clay the $\delta^{13}C_{org}$ data document a decrease to values around -26.9 ‰ at 525.07 m. When crossing the lithological boundary, the first sample at 524.50 m already documents a significant jump to higher values around -25.8 ‰, which is around 1 ‰ more positive than beneath. These positive values lead over into the lower part of the Wedelsandstein Formation where they rise even further to values at -25.2 ‰ at 512.00 m and 510.00 m. The interval from 509.00 m to the top of the cored interval (sample at 499.12 m) is again slightly shifted to more negative values (-25.9 ‰ at 509.00 m) but still show a positive trend to the top, reaching -25.5 ‰.

The TOC reflects the different lithologies between the three formations. In the uppermost Opalinus Clay the TOC increases from 0.8 wt.-% (540.06 m) through the following 15 m and reaches double in the top half metre (1.6 wt.-% at 525.07 m). The above-mentioned sample at

531.00 m, just above the uppermost calcareous marl bed (532.25 – 531.97 m), also documents a change in the lithology during this trend. The TOC below and above are clearly different with higher TOC values in the interval above. The three analysed samples from the «Murchisonae-Oolith Formation» show an intermediate state (TOC around 0.8 wt.-%) before reaching the Wedelsandstein Formation with very low TOC values (< 0.5 wt.-%). The lithological boundaries (524.61 m and 521.43 m) clearly document the horizons where the change in the TOC happened.

The C/N ratios show a minor increasing trend in the upper part of the «Sub-unit with silty calcareous beds» which continues in the above following formation. The ratio starts at 540.06 m with 18 and reaches two higher values: one at 531.00 m with 22 and an upper one at 525.07 m with 23. In the lowermost Wedelsandstein Formation the ratio decreases from 18 at 521.37 m to 13 at 518.00 m. Afterwards the ratio increases again slightly to the uppermost part of the cored interval. The uppermost sample, taken at 499.12 m, has a C/N ratio of 32, which is outside the range shown in Fig. 3-3 and most likely does not reflect a reliable ratio.
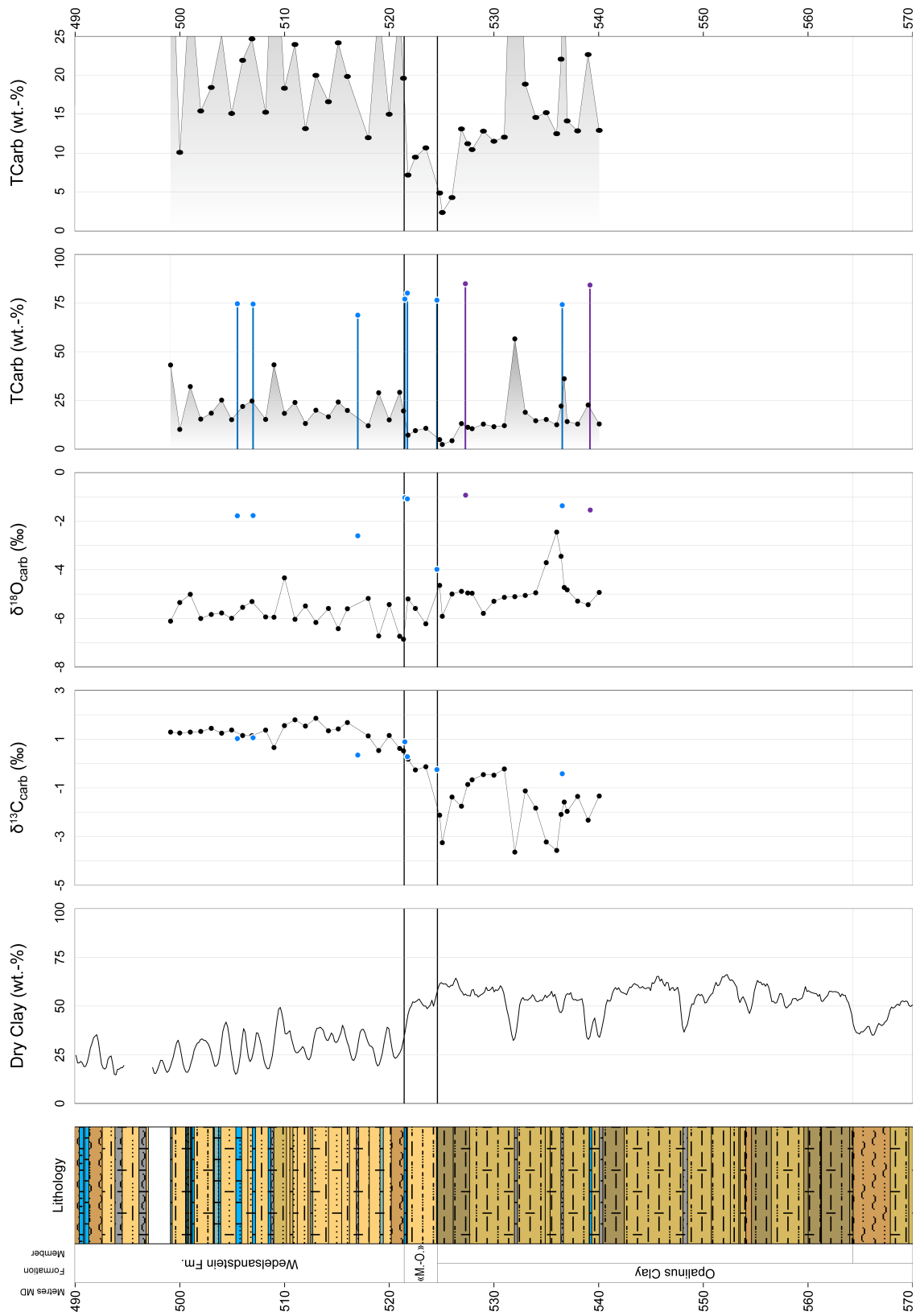
Fig. 3-2: Bulk rock (carbonate) isotopic data from the Dogger Group

Geochemical data from 540.06 – 499.12 m, additional explanations and references see text at the beginning of Section 3.4.
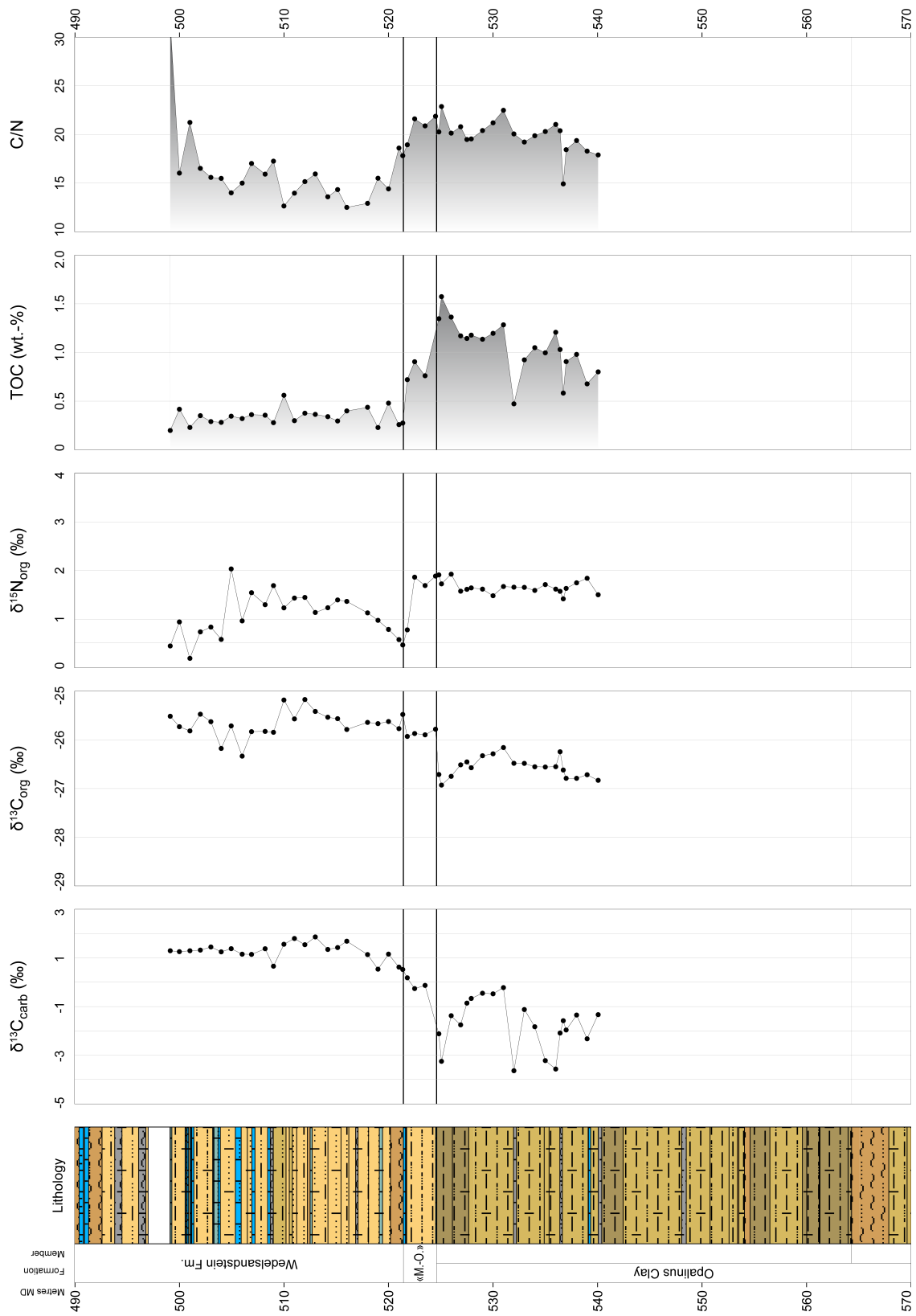
Fig. 3-3:   Organic isotopic data from the Dogger Group

Geochemical data from 540.06 – 499.12 m, additional explanations and references see text at the beginning of Section 3.4.

4 Definition of specific lithostratigraphic boundaries

The boundaries between stratigraphical units, as also shown in the stratigraphical logs of the litho-stratigraphy report (Dossier III), were mostly defined by using lithological criteria. According to the guidelines on stratigraphical nomenclature of Remane et al. (2005), the definition of litho-stratigraphical units should be based, both vertically and horizontally, on lithological variations regardless of their age. In fact, the formation boundaries, as used by Nagra for the ongoing bore-hole campaign of Stage 3 of the Sectoral Plan for Geological Repositories (Jordan & Deplazes 2019), were not always obvious in the borehole and definitions were difficult to apply, either because of the small core diameter or because of differences in facies. The exact location of some of the formation boundaries caused discussions during core description and the process of quality control. Most of the important data for questionable boundaries were already present before the data-freeze (07.01.2022) and were used for the log descriptions and drawings. In the following paragraphs, the underlying considerations are explained for providing a better understanding of how boundaries were demarcated. We are aware of the fact that the upper boundaries of the Opalinus Clay and the «Murchisonae-Oolith Formation» are no longer based on lithological criteria alone and that chronostratigraphic criteria (ammonite, palyno- and chemostratigraphy) are included in the definitions.

Opalinus Clay (668.07 – 524.61 m)

The *lower boundary* of the Opalinus Clay was not part of the investigated interval in this report. It was set at 668.07 m at the top of the uppermost calcareous marl of the Staffelegg Formation (*cf.* Dossier III).

The *upper boundary* of the Opalinus Clay is set at 524.61 m at the base of the overlying 10 cm thick interval enriched in encrusted limestone intraclasts with iron-ooids and bioclasts (*cf.* Dossier III). Placing the boundary at this level was not based on lithological reasons alone. But the close lithological relation with MAR1-1 led to place the boundary at the same location (e.g. Jordan et al. 2021, Wohlwend et al. 2021b). Placing the boundary in MAR1-1 at that level was also done by a comparison with the newly established stratigraphy in the Benken borehole (Bläsi et al. 2013), where the palynological sample, taken directly from the hardground, has given already an age from the Bradfordensis Zone which is identical to the palynological sample at 590.38 m in MAR1-1 (Wohlwend et al. 2021b). The similar change in the palynological assemblages is also documented in RHE1-1. The sample from the top of the Opalinus Clay (524.82 m) is interpreted as Opalinum Zone, probably Bifidatum Subzone. The sample just above at 524.27 m points with the co-occurrence of *Nannoceratopsis triangulate*, *Scriniocassis weberi* (both LADs at the top of the Opalinum Zone), questionable *Evansia*? *spongogranulata* (FAD in the Murchisonae Zone) and a few single specimens of questionable *Dissiliodinium* spp. (FAD within the Bradfordensis Zone) to a possible natural mixing of assemblages of different ages (Opalinum, Murchisonae and Bradfordensis Zones) due to condensation and/or reworking.

The positive chemostratigraphic shift or even jump with an amplitude of around +1 ‰ in the $\delta^{13}C_{org}$ values to average values above -26.0 ‰ (*cf.* Wohlwend et al. 2021a and 2021b) occurs in that interval too (524.82 m = -26.7 ‰ and at 524.50 m = -25.8 ‰; Fig. 3-3). The C-isotope jump also indicates a larger temporal gap, or condensation between the two above-mentioned samples. The slightly enriched $\delta^{13}C_{org}$ value at 531.00 m (-26.2 ‰), just above the uppermost calcareous bed (532.25 – 531.97 m) may be linked to the positive shift (e.g. BUL1-1 at around 899.00 m; Wohlwend et al. 2021a) which seems to be typical for the Bifidatum Subzone of the Opalinum Zone.

«Murchisonae-Oolith Formation» (524.61 – 521.43 m)

The *lower boundary* of the «Murchisonae-Oolith Formation» is set at 524.61 m at the base of the 10 cm thick interval enriched in encrusted limestone intraclasts with iron-ooids (*cf.* Dossier III). The thin section taken from that interval (RHE1-1-524.57) documents a microfacies which is typical for an iron-oolite (42 vol.-% iron-ooids) whereas most of the iron-ooids are replaced by calcite, but many have retained their ferruginous core (see also Fig. B-4 in Appendix B). Detailed discussion about the boundary and the age constrain can be found above at the upper boundary of the Opalinus Clay.

The *upper boundary* of the «Murchisonae-Oolith Formation» is set at 521.43 m at the top of the upper condensed section (521.79 – 521.43 m) with encrusted and bored intraclasts forming four nodular beds (*cf.* Dossier III). Placing the boundary at this level was not based on lithological reasons alone. But the close lithological relation with MAR1-1 led to place the boundary at the same location (e.g. Jordan et al. 2021, Wohlwend et al. 2021b). In MAR1-1 the ammonite finding directly on the hardground (589.19 m: *Staufenia* ex gr. *staufensis*) belongs clearly to the Bradfordensis Subzone of the Bradfordensis Zone, which is also confirmed by the palynological samples (Wohlwend et al. 2021b). The lithological comparison with Benken and the newly established stratigraphy therein (Bläsi et al. 2013) shows the same expression. Therefore, the same approach was chosen in RHE1-1 and the lithological boundary was set on top of the uppermost hardground at 521.43 m. The palynological sample from the base of this condensed section at 521.79 m is dated questionably Opalinum Zone to questionably Bradfordensis Zone, although the sample taken 6 cm above the condensed bed at 521.37 m is already defined by the first occurrence of *Dissiliodinium giganteum* having the FAD in the Ovale Zone. The ammonite (Graphoceratidae indet.) found in-between at 521.54 m yields an age of probably Concavum Zone to earliest Discites Zone.

The biostratigraphic findings in Benken, MAR1-1 as well as now in RHE1-1 document a hardground building during the Bradfordensis Zone and probably a very condensed sedimentation during the Concavum to Discites Zone. The onset of the sedimentation of the hanging Wedelsandstein Formation started again in the Ovale Zone. The «Sowerbyi-Oolith», which by definition would be the base of the Wedelsandstein Formation (German Stratigraphic Scheme; Bloos et al. 2005), is most likely absent or amalgamated in the uppermost few centimetres of this condensed section between 521.79 m to 521.43 m.

Wedelsandstein Formation (521.43 – 482.8 m)

The *lower boundary* of the Wedelsandstein Formation is set at 521.43 m just above the condensed section with several hardgrounds (521.79 – 521.43 m) (*cf.* Dossier III). The onset of the sedimentation of the Wedelsandstein Formation started in the Ovale Zone (palynological sample at 521.54 m). Detailed discussion about the boundary and a comparison with MAR1-1 can be found above at the upper boundary of the «Murchisonae-Oolith Formation».

The *upper boundary* of the Wedelsandstein Formation was not cored in RHE1-1, coring started at 499.10 m. The lithological boundary was placed at 482.8 m by the onset (or disappearance from top to bottom) of iron-ooids, which are typically for the above following formation and by a concurrent sharp increase in the resistivity in the FMI log to the above following succession (*cf.* Dossier III).

5   Conclusion

The present study documents data on microfacies analysis, ammonite stratigraphy and palyno-stratigraphy as well as detailed geochemical analyses (C, O and N isotopes) on the transition from Opalinus Clay to Wedelsandstein Formation. With this data collection, it was possible to predict the delimitation of these formations more accurately. Most of the important data for the boundaries in question were already present at the data-freeze (07.01.2022). Therefore, the present report complements the lithostratigraphic report of Dossier III for the deep borehole Rheinau-1-1. The lithological boundaries, and therefore the stratigraphic profile, were mostly defined by lithological criteria. Nevertheless, the customary formal and informal formation boundaries were not always obvious in the drill cores, either because of the small core diameter or changing facies conditions. The exact location of specific formation boundaries led to discussions requiring additional data to determine the exact profile description and illustration. We are aware that certain boundaries are thus no longer based solely on lithological criteria, and that the definitions therefore also include chronostratigraphic criteria (ammonite stratigraphy, palyno- and chemostratigraphy).

6 References

Bathurst, R.G.C. (1975): Carbonate sediments and their diagenesis (2nd ed.), Developments in Sedimentology, Amsterdam, Elsevier, 658 pp.

Birkhäuser, P., Roth, P., Meier, B. & Naef, H. (2001): 3-D Seismik: Räumliche Erkundung des mesozoischen Sedimentschichten im Zürcher Weinland. Nagra Technical Report NTB 00-03.

Bläsi, H.R., Deplazes, G., Schnellmann, M. & Traber, D. (2013): Sedimentologie und Stratigraphie des 'Braunen Doggers' und seiner westlichen Äquivalente. Nagra Arbeitsbericht NAB 12-51.

Bloos, G., Dietl, G. & Schweigert, G. (2005): Der Jura Süddeutschlands in der Stratigraphischen Tabelle von Deutschland 2002. Newsletters on Stratigraphy 41, 263-277.

Cariou, E. & Hantzpergue, P. Coord. (1997): Biostratigraphie du Jurassique ouest-européen et méditerranéen: zonations parallèles et distribution des invertébrés et microfossiles. Bull. Centre Rech. Elf Explor. Prod.

Dickson, J.A. (1965): Modified staining technique for carbonates in thin section. Nature 205, 587.

Dietze, V., Gräbenstein, S., Franz, M., Schweigert, G. & Wetzel, A. (2021): The Middle Jurassic Opalinuston Formation (Aalenian, Opalinus Zone) at its type locality near Bad Boll and adjacent outcrops (Swabian Alb, SW Germany). Palaeodiversity 14/1, 15-113.

Emerson, S. & Hedges, J.I. (1988): Processes controlling the organic carbon content of open ocean sediments. Paleoceanography 3, 621-634.

Feist, S. (1987): Palynologische Untersuchungen im Braunjura beta und unteren Braunjura gamma (oberes Aalenium bis unteres Bajocium) der Bohrungen Hausen, nordöstliche Schwäbische Alb. Diploma Thesis, University of Tübingen. 78pp.

Feist-Burkhardt, S. & Pross, J. (2010): Dinoflagellate cyst biostratigraphy of the Opalinuston Formation (Middle Jurassic) in the Aalenian type area in southwest Germany and north Switzerland. Lethaia 43, 10-31.

Fernandez, A., van Dijk, J., Müller, I.A. & Bernasconi, S.M. (2016): Siderite acid fractionation factors for sealed and open vessel digestions at 70°C and 100°C. Chemical Geology 444, 180-186.

Isler, A., Pasquier, F. & Huber, M. (1984): Geologische Karte der zentralen Nordschweiz 1:100'000. Herausgegeben von der Nagra und der Schweiz. Geol. Komm.

Jäggi, D., Laurich, B., Nussbaum, C., Schuster, K. & Connolly, P. (2017): Tectonic structure of the "Main Fault" in the Opalinus Clay, Mont Terri rock laboratory (Switzerland). Swiss Journal of Geosciences 110, 67-84.

Jordan, P. & Deplazes, G. (2019): Lithostratigraphy of consolidated rocks expected in the Jura Ost, Nördlich Lägern and Zürich Nordost regions. Nagra Arbeitsbericht NAB 19-14.

Jordan, P. Schürch, P. Naef, H., Schwarz, M., Felber, R., Ibele, T. & Gysi, M. (2021): TBO Marthalen-1-1: Data Report. Dossier III. Lithostratigraphy. Nagra Arbeitsbericht NAB 21-20.

Kukal, Z. (1971): Geology of recent sediments. Academie Press, New York, 490 pp.

Nagra (2014): SGT Etappe 2: Vorschlag weiter zu untersuchender geologischer Standortgebiete mit zugehörigen Standortarealen für die Oberflächenanlage. Geologische Grundlagen. Dossier II: Sedimentologische und tektonische Verhältnisse. Nagra Technical Report NTB 14-02.

Nagra (2019): Preliminary horizon and structure mapping of the Nagra 3D seismics ZNO-97/16 (Zürich Nordost) in time domain. Nagra Arbeitsbericht NAB 18-36.

Ogg, J.G., Ogg, G. & Gradstein, F.M. (2016): The Concise Geologic Time Scale. Cambridge University Press. 184 pp.

Parsons, T.R. (1975): Particulate organic carbon in the sea. *In*: Riey, J.P. & Skirrow, G. (eds.): Chemical oceanography. Academie Press, London, 338-425.

Pietsch, J. & Jordan, P. (2014): Digitales Höhenmodell Basis Quartär der Nordschweiz – Version 2013 (SGT E2) und ausgewählte Auswertungen. Nagra Arbeitsbericht NAB 14-02.

Remane, J., Adatte, T., Berger, J.P., Burkhalter, R., Dall'Agnolo, S., Decrouez, D., Fischer, H., Funk, H., Furrer, H., Graf, H.R., Gouffon, Y., Heckendorn, W. & Winkler, W. (2005): Richtlinien zur stratigraphischen Nomenklatur. Eclogae geol. Helv. 98/3, 385-405.

Roche, V., Childs, C., Madritsch, H. & Camanni, G. (2020): Controls of sedimentary layering and structural inheritance on fault zone structure in three dimensions. A case study from the northern Molasse basin, Switzerland. Journal of the Geological Society 177/3, 493-508.

Scheffer, F. & Schachtschnabel, P. (1984): Lehrbuch der Bodenkunde. Enke Verlag, Stuttgart.

StrataBugs, version 2.1 (June 2016): StrataData Ltd., UK. http://www.stratadata.co.uk.

Timescale Creator, version 7.0 (30. July 2016): Geologic TimeScale Foundation. https://engineering.purdue.edu/Stratigraphy/tscreator/.

Voigt, E. (1968): Über Hiatus-Konkretionen (dargestellt an Beispielen aus dem Lias). Geologische Rundschau 58, 281-296.

Wetzel, A. & Allia, V. (2000): The significance of hiatus beds in shallow-water mudstones: an example from the Middle Jurassic of Switzerland. Journal of Sedimentary Research 70/1, 170-180.

Wohlwend, S., Hart, M. & Weissert, H. (2016): Chemostratigraphy of the Upper Albian to mid-Turonian Natih Formation (Oman) – how authigenic carbonate changes a global pattern. The Depositional Record 2/1, 97-117.

Wohlwend, S., Bernasconi, S.M., Deplazes, G. & Jaeggi, D. (2019): SO Experiment: Chemostratigraphic study of Late Aalenian to Early Bajocian. Mont Terri Technical Report TR 19-05. Federal Office of Topography (swisstopo), Wabern, Switzerland.

Wohlwend, S., Bläsi, H.R., Feist-Burkhardt, S., Hostettler, B., Menkveld-Gfeller, U., Dietze, V. & Deplazes, G. (2021a): TBO Bülach-1-1: Data Report – Dossier IV: Microfacies, Bio- and Chemostratigraphic Analysis. Nagra Arbeitsbericht NAB 20-08.

Wohlwend, S., Bläsi, H.R., Feist-Burkhardt, S., Hostettler, B., Menkveld-Gfeller, U., Dietze, V. & Deplazes, G. (2021b): TBO Marthalen-1-1: Data Report – Dossier IV: Microfacies, Bio- and Chemostratigraphic Analysis. Nagra Arbeitsbericht NAB 21-20.

Wood, G.D., Gabriel, A.M. & Lawson, J.C. (1996): Palynological techniques – processing and microscopy. *In*: Jansonius, J. & McGregor, D.C. (eds.): Palynology, principles and applications. American Association of Stratigraphic Palynologists Foundation 2, 29-50.

Appendix A: List of all samples

Appendix A1: List of all thin sections from RHE1-1 (561.26 – 500.75 m)

For the description and individual counting of the thin sections see Section 3.1; selected photos can be found in Appendix B.

Top [m]	Bottom [m]	Avg. depth [m]	Formation	Retrieval date [dd.mm.yyyy]	Sample ID
500.73	500.77	500.75	Wedelsandstein Fm.	07.12.2021	RHE1-1-500.75-TS
505.86	505.90	505.88	Wedelsandstein Fm.	07.12.2021	RHE1-1-505.88-TS
521.45	521.49	521.47	«Murchisonae-Oolith Fm.»	07.12.2021	RHE1-1-521.47-TS
524.50	524.54	524.52	«Murchisonae-Oolith Fm.»	07.12.2021	RHE1-1-524.52-TS
524.55	524.59	524.57	«Murchisonae-Oolith Fm.»	07.12.2021	RHE1-1-524.57-TS
536.58	536.62	536.60	Opalinus Clay	07.12.2021	RHE1-1-536.60-TS
548.39	548.43	548.41	Opalinus Clay	07.12.2021	RHE1-1-548.41-TS
561.24	561.28	561.26	Opalinus Clay	07.12.2021	RHE1-1-561.26-TS

Appendix A2: List of the sampled ammonite from RHE1-1 (521.54 m)

For the definitive determination of the ammonite see Section 3.2 (Tab. 3-2).

Top [m]	Bottom [m]	Sample depth [m]	Formation	Retrieval date [dd.mm.yyyy]	Sample ID
521.51	521.56	521.54	«Murchisonae-Oolith Fm.»	07.12.2021	RHE1-1-521.54-BS(MF)

Appendix A3: List of other provisionally determined conspicuous macrofossils from RHE1-1 (677.48 – 651.45 m)

Top [m]	Bottom [m]	Fossil	Determination (provisional)
651.45		Ammonite	*Leioceras subglabrum*
651.50	653.19	Ammonites	*Leioceras* ex gr. *opalinum*
653.58		Ammonite	*Leioceras opalinum*
655.16		Ammonite	*Leioceras* ex gr. *subglabrum*
663.67		Ammonite	*Leioceras* ex gr. *subglabrum*
667.61		Ammonite	*Pleydellia* ex gr. *buckmani*
670.01		Ammonite	*Pleydellia* sp.
671.46		Ammonite	*Dumortieria*
672.75		Ammonite	*Perilytoceras jurense*?
674.70		Ammonite	*Perilytoceras jurense*?
677.16		Wood	wood
677.48		Wood	wood
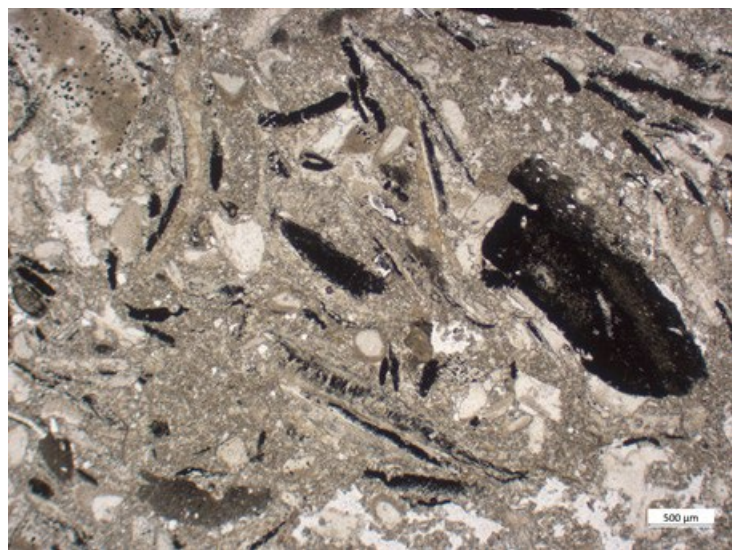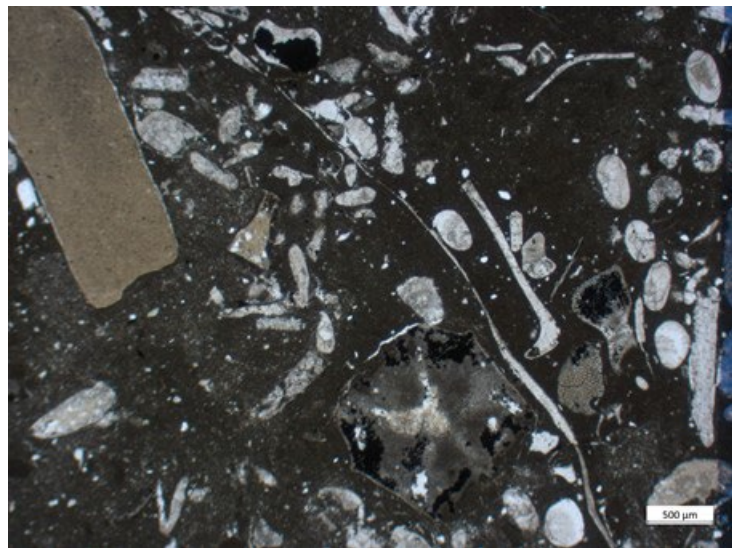
Appendix A4:   List of all palynological samples from RHE1-1 (540.06 – 499.12 m)

Top [m]	Bottom [m]	Avg. Depth [m]	Formation	Retrieval date [dd.mm.yyyy]	Sample ID
499.10	499.13	499.12	Wedelsandstein Fm.	05.10.2021	RHE1-1-499.12-BS(PA)
504.93	504.96	504.95	Wedelsandstein Fm.	05.10.2021	RHE1-1-504.95-BS(PA)
515.11	515.14	515.13	Wedelsandstein Fm.	05.10.2021	RHE1-1-515.13-BS(PA)
521.35	521.38	521.37	Wedelsandstein Fm.	05.10.2021	RHE1-1-521.37-BS(PA)
521.78	521.80	521.79	«Murchisonae-Oolith Fm.»	05.10.2021	RHE1-1-521.79-BS(PA)
524.25	524.28	524.27	«Murchisonae-Oolith Fm.»	05.10.2021	RHE1-1-524.27-BS(PA)
524.80	524.83	524.82	Opalinus Clay	05.10.2021	RHE1-1-524.82-BS(PA)
527.25	527.27	527.26	Opalinus Clay	05.10.2021	RHE1-1-527.26-BS(PA)
531.49	531.51	531.50	Opalinus Clay	05.10.2021	RHE1-1-531.50-BS(PA)
536.41	536.43	536.42	Opalinus Clay	05.10.2021	RHE1-1-536.42-BS(PA)
536.72	536.74	536.73	Opalinus Clay	05.10.2021	RHE1-1-536.73-BS(PA)
540.04	540.07	540.06	Opalinus Clay	05.10.2021	RHE1-1-540.06-BS(PA)
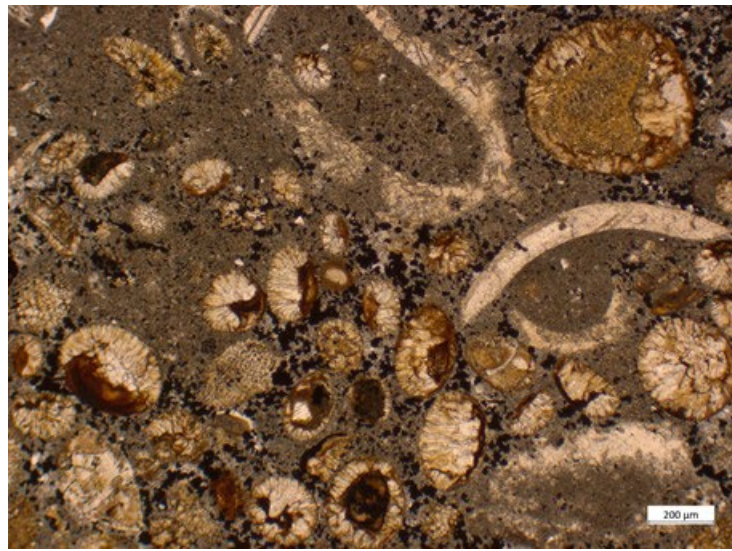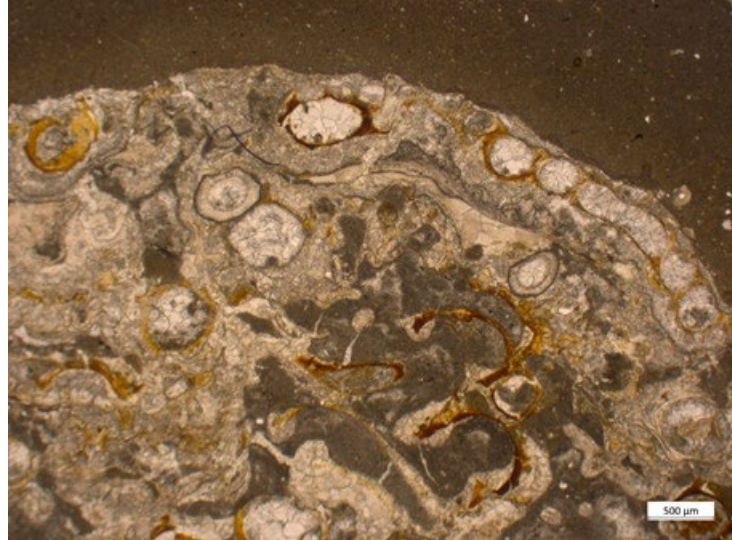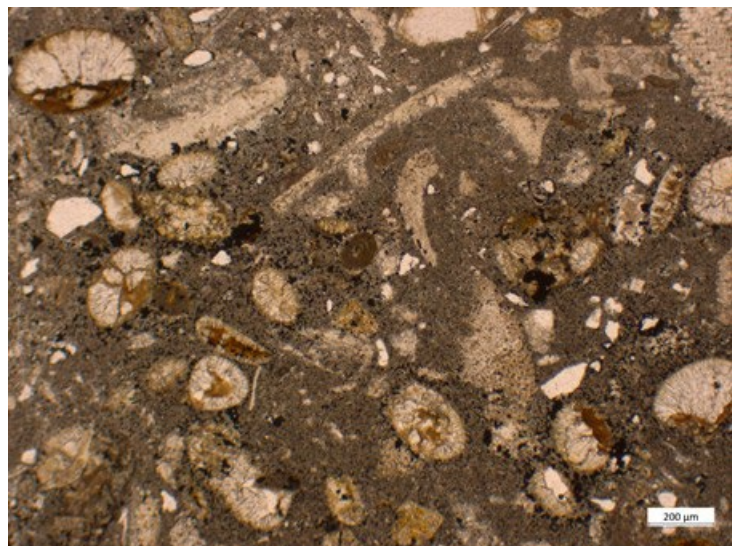
Appendix B: Photos microfacies

Fig. B-1:

Bioclastic calcareous marl to limestone (argillaceous): the main components are pyrite-rich bivalves and pyrite-rich intraclasts

Thin section photo

RHE1-1-561.26
Opalinus Clay

Fig. B-2:

Iron-oolitic and sideritic, bioclastic calcareous marl, composed of calcitic iron-ooids, bioclasts and intraclasts, surrounded by a sideritic, marly matrix

Thin section photo

RHE1-1-548.41
Opalinus Clay

Fig. B-3:

Sideritic, bioclastic calcareous marl with micritic nodules (upper left and bottom right corner). The upper nodule shows an irregular wavy outline, generated by the growth of the nodule during diagenesis

Thin section photo: right half stained for calcite = red

RHE1-1-536.60
Opalinus Clay

Selected photos of microfacies from Opalinus Clay

Fig. B-4:

Iron-oolite with many iron-ooids, whereof most are replaced by calcite, except their ferruginous or limonitic core.

Thin section photo

RHE1-1-524.57
«Murchisonae-Oolith Fm.»

Fig. B-5:

Special biogenic crust, fixed underneath of a micrite intraclast (top part)

Thin section photo

RHE1-1-524.52
«Murchisonae-Oolith Fm.»

Fig. B-6:

Iron-oolitic, bioclastic limestone (sandy): calcitic iron-ooids, bioclasts, quartz sand, pyrite and micritic matrix

Thin section photo

RHE1-1-521.47
«Murchisonae-Oolith Fm.»

Selected photos of microfacies from «Murchisonae-Oolith Fm.»

Appendix C: Palynostratigraphy

Appendix C1:   Range Chart: Quantitative stratigraphic distribution of Middle Jurassic palynomorphs in the Rheinau-1-1 borehole

Appendix C2:   Depth/Age plot: Rheinau-1-1 borehole

Note: The appendices are only included in the digital version of this report (PDF) and can be found under the paper clip symbol.

Appendix D: Chemostratigraphy

Appendix D1:   List of all geochemical samples and results mainly drilled from specific calcareous beds in the Opalinus Clay and its overlying confining unit

Data are discussed in Section 3.4 and partly illustrated in Fig. 3-2 (part of the data points lie outside the presented scale for the $\delta^{13}C_{carb}$). The sample taken at 655.02 m is coming from the lower part of the Opalinus Clay and is therefore not shown on Fig. 3-2: HB: drilled from a "hiatus bed" (for definition of HB see Section 2.1), SN: drilled from a septarian nodule, TS: drilled directly from thin section sample (see microfacies description in Section 3.1).

Depth [m]	Description of sample		TS	$\delta^{13}C_{carb}$ [‰ VPDB]	$\delta^{18}O_{carb}$ [‰ VPDB]	Carbonate [wt.-%]
505.50	Bioclastic limestone (sandy)			1.03	-1.78	74.6
507.00	Limestone (argillaceous & sandy)			1.06	-1.77	74.5
517.00	Calcareous marl (sandy)			0.35	-2.60	68.8
521.50	Bioclastic limestone (iron-oolitic)			0.89	-1.04	77.0
521.74	Bioclastic limestone (iron-oolitic)			0.28	-1.09	80.1
524.56	Micritic intraclasts with iron-ooids		×	-0.25	-3.98	76.5
527.30	Septarian nodule	SN		-16.94	-0.93	85.0
536.53	Bioclastic marl with micritic nodules	HB		-0.42	-1.37	74.2
539.20	Septarian nodule	SN		-16.96	-1.54	84.3
655.02	Septarian nodule	SN		-23.07	-1.62	82.4